Author final response

Dear Editor, Dear Reviewer #1 and Reviewer #2,

thank you very much for spending the time to carefully review the manuscript and for your constructive comments to improving the paper. We carefully revised the paper and considered all points as listed below (equivalent to the final response). Please find also attached a latexdiff document which shows all changes made to the manuscript.

Below are all referee comments (**RC**) by Referee **#1** and Referee **#2** and the corresponding author comments (**AC**). Suggested changes in the manuscript are indicated by *italic* words.

Main changes are

- Removal of the single-image detection which did not provide new insight.
- The essay about meteorological conditions was replaced by a reference.
- A quantitative analysis of the avalanche size distribution was added (see figure).
- The discussion of the multiorbital composites were improved.

The two removals (as suggested by Reviewer **#2**.) shorten the body manuscript which, however, was balanced in length by adding additional information (size distribution, additional discussion). Therefore we will try to shorten the manuscript wherever possible.

Author response to reviewer #1:

General comments

RC1: The paper describes (...). It analyzes (...) and cross compares(...). The paper is interesting and well organized (...) of high interest for the scientific community(...).

AC1: Thank you very much for this positive feedback.

RC1.1: *cont. general comment*
The only flaw, honestly declared by the authors, is the lack of a real comparison with a ground truth which in the studied case is practically impossible.

AC1.1: Yes, the study was based on archive TSX data and such avalanche events can only be predicted very few days in advance. Therefore it was impossible to schedule any ground truth campaigns. We are currently working on a follow-up study which will evaluate if operationally acquired ground based data could be used for ground truth.

RC1.2: *cont. general comment*
A minor issue of the dataset is also the revisit time of the analyzed satellites that, obviously, is not synchronized with main avalanche event but it is widely balanced by the possibility of carrying out an avalanche mapping of entire country like Switzerland (Figure 9 is really impressive when zoomed).

AC1.2: This might be a misunderstanding but scene selection was indeed not simple. The area of TSX images was defined by available data from the archived data *synchonized* with the two avalanche events. Then, S1 images were *synchonized* by time in incidence angle with the TSX data. The image selection to cover entire Switzerland was defined by the first avalanche event. Unfortunately, TSX data for the second period did not well match the acquisition date of the SPOT-6 images.

To clarify that we did our best to *synchronize* the satellite acquisitions we will modify section 2:
For TSX, no systematic coverage is available *over Switzerland* because TSX acquires data upon request. (...) To cover the two extreme avalanche events around Jan 4th and 22nd 2018 (Fig. 2) with images acquired from identical orbits *as good as possible* we searched the archive for a sequence of images which limited the study area to the Alps of Uri in central Switzerland. *The orbit repeat time defines the dates and limits the revisit time to 11 d for the first event and 22 d for the second one (one missing acquisition).* The Sentinel-1 images were carefully selected to cover the first main avalanche event. We suggest to add to section 2: *To study the possibility of detecting avalanches for entire Switzerland for the first avalanche event, S1 acquisitions were carefully selected from multiple orbits during a 5 day period with from before and after the first event (Table A1).*

Specific comments

RC2: The experiment was carried out in a zone featuring a high avalanche activity. It would be interesting, at least at discussion level, to evaluate the performance of the proposed approach in a low frequency area, i.e. to test the capability to detect few sparse events.

AC2: The first criterion to detect avalanches is a brightness threshold of 4 dB which is better fulfilled as long as no new avalanches overlap with old ones. That means that sparse events are more likely to detected than overlapping avalanches in densely avalanche-covered areas. A later criterion is that avalanches must have a certain size to be detected which efficiently filters out noise in areas with sparse events. To address these two point, we suggest to add after the first sentence in section 6.5 (discussion: automated avalanche detection):
For both, TSX and S1 images the implemented avalanche detection algorithm performs with reasonable results, at least when the number of overlapping avalanches is low. *That means that a few sparse events are more likely to be detected than overlapping clusters of avalanches.*

RC3: Figure 2 is really interesting and deserves an improvement for the sake of readability. As the investigated time span is only a fraction of the plotted graph. Maybe a zoomed plot could be added beside the current one. In the main plot only the AAI and the avalanche type time series should be plotted. In the second, zoomed, one also satellites acquisitions should be added, possibly on a secondary x-axis on top of the plot.

AC3: Thanks for this suggestion. Honestly, I spent multiple days working on this figure and I tried already (before submission) to improve the figure in the direction suggested by you. However, I was not satisfied with the solution main+subplot because to show the intensity of the two extreme events on 2018-01-04 and 2018-01-22 the y-axis of the graph should not be cut more than it already is (AAI = 1200). Zooming to the study period late December - early February leaves no space for the legend and y-axis label; furthermore, a zoomed sub-graph would require a lot of vertical space when not cutting of the y-axis. I think the readability will *appear* improved in the two-column format (without changing the size) because then it fills the full width of one of the two columns. I agree, that in the 1-column manuscript, where it is displayed with half page width, it appears a bit small.

RC4: Line 134. I guess the topographic relief map is the same used for orthorectification, i.e SwissAlti3D. It would be better to specify it.

AC4: Yes, we used the Alti3D for that evaluating the flow path in single-image avalanche detection. However, we like to follow the suggestion of Reviewer **#2** to remove the results and discussion about single-image detection. According to Reviewer **#2**, there is no point to evaluate a technique which is behind the state-of-the-art of two-image change detection.

Technical corrections

RC5: Technical corrections In figures 4-8,11, A2, A3 the scale bar is too close to its outline, please increase the distance.

AC5: done.

RC6: In figure 6-8,11, A2, A3 the line fill masks the readability of detected avalanches.

AC6: The idea of these images is to show and compare the masks. - Figure 6 will be removed as suggested by Reviewer #2.
- The sole purpose of Figure 7 is to compare masks. Even when the line fill masks would be removed and only an outline would be used to show the avalanche area, the outline would either bias the reader or mask the avalanche edge (for the optical image 7).
- For Fig. 8 we will add to the caption that *the S1 image in the background is shown without mask in Fig. 4c*.
- The same holds for Fig. 11 (TSX) which is already shown in Fig. 4b without mask.
- In Figure A2 and A3, the relatively large spaces between the line fill mask make it possible to see the backscatter image when zooming in.

RC7: (typos)
Line 18. moasic –>mosaic
Line 101. scatters –>scatter
Line 367. reduces –>reduced

AC7: Thanks; all typos have been corrected.

Author response to reviewer #2:

General comments

RC8: Overall the manuscript is sound and very well written (...). The biggest problems I see, actually, are that some of the content might not be relevant and the manuscript could potentially be shortened.

AC8: We will consider your suggestions and will remove the single-avalanche detection (reduces the manuscript length by 2 pages and 2 figures) and will replace the description of meteorological event (1/2 page) by a reference. (See RC8.1/24 and RC16).

RC8.1: I do not see much value in presenting detection in single backscatter images.

AC8.1: See **AC8** and **RC24**. We will remove the single backscatter analysis. This will shorten the manuscript by almost 2 pages and will also remove 2 figures.

RC8.2: although beautiful to look at, I do not see much value in the multiorbital composite, especially not for automatic detection.

AC8.2: This contradicts a bit RC26 "very impressive", doesn't it? We like explicitly point out here the three main advantages of multiorbital composites:

+ the reduction of invisible areas (mainly layover).
+ the enhancement of resolution for near-layover areas.
+ the reduction of radar speckle noise.

However, there are also some apparent disadvantages of the multiorbital composites which we will discuss in the manuscript (see also RC31):

- *loosing some temporal resolution (when the time difference between asc+desc acquisitions is large). Under unfortunate cases, when avalanches occur between the averaged acquisitions, they appear half as bright and are more likely to be missed. However, the less time elapses between asc and desc acquisitions the more likely it is that avalanches are captures with both orbits which improves the SNR for detection. In our study, acquisitions were carefully selected to best image the avalanches of the first avalanche event on 2018-01-04.* We will add this information to the discussion of the multiorbit composites and will mention also in the conclusion *that especially the ratio between the elapsed time between asc and desc acquisition and the revisit-time must be minimized.*

We think the above disadvantage is only *apparent*, because we draw important conclusions from the multiorbit averaging which hint in the direction that local resolution weighting (Small, 2012) will further improve our results (and reduces the effect of loosing temporal resolution) we will add to the discussion: *In mountaineous regions, LRW applies already unequal weights for ascending and descending acquisitions which further decreases the probability that avalanche visibility is reduced by the multiorbital averaging.*

While reconsidering the advantage of the multiorbital composites we also realized that *shadow areas are not improved because they are located in layover when imaged from the opposite orbit.*

Specific comments

RC9: Figure 1: there is no black rectangle.

AC9: It's in the inset. We will modify the figure caption to: *The black rectangle in the insets shows the full footprint of the TSX scene over Switzerland.*

RC10: Table 1: could you also indicate orbit number and geometry (asc/desc)?

AC10: sure.

RC11: line 53: 55x35 km2, that does not seem correct.

AC11: This number was measured from the scene extent. It is close to the standard footprint size of TSX in single-pol stripmap mode. We will hint to the *inset of Fig. 1* which shows the size of the footprint to avoid misunderstanding.

See also **RC13** "Why the square?": When specifying an area I think the correct unit should be km^2. It might seem a bit awkward to write $55 \times 35\ \text{km}^2$ but in my opinion it's the best way to specify the extent. Alternative formulations would be 55 km $\times$35 km or 1925 km^2 (I have not found any standards for areas in NHESS).

RC12: line 57: where did you download since you had to wait 24 h?

AC12: This might be a misunderstanding: for this study we did not analyze any time-critical data and did not had to wait. The 24 h describe the general availability of S1 data. As the current reference does not contain this information, we will update the reference where this information is provided: "Global products will be systematically generated for all acquired data. (...) These products are made available (...) in any case within 24 h after observation." (ESA, 2012, p.35). See also https://sentinel.esa.int/web/sentinel/missions/sentinel-1/data-distribution-schedule

RC13: line 59: same as line 53. why the square?

AC13: See **AC11**.

RC14: Figure 2: could you add some more details on the AAI. if I understand it correctly, this is the AAI for entire SUI? From which observations is it calculated (no need to tell us how).

AC14: I will add to the caption: *The avalanche activity index is the weighted sum of all reported avalanches for Switzerland (Schweizer et al., 2003, 1998).* The AAI depends on visibility, because avalanches can only be *reported* when visible for a human observer.

RC14.1: What does mixed snow mean (dry high up, wet in the valleys, or due to aspect)?

AC14.1: We'll add to the caption: *"mixed snow" indicates dry snow avalanches which started high up but were slowed down at medium altitude by wet snow.*

RC15: Figure 2: why are the dates of the multiorbital S1 images not shown in Table 1? ok see them in table A1 now!

AC15: We will add the reference to table A1 to the caption of table 1 and Fig. 2.

RC16: section 2.1: in case you feel like your article is too long, I think this section could be deleted or shortened substantially. You could refer to Yves paper or the SLF special report.

AC16: We'll delete this section and refer in Sect. 2 to Yves paper (Bühler et al., 2019) instead. We do anyway not refer to this section in the remainder of the paper.

RC17: line 85: dry slab avalanches at least have three different zones. In case of very wet slab avalanches the zones are more diffuse and in case of loose snow avalanches I would say they are absent.

AC17: Thanks for noting this. We will reformulation the sentence to *Fig. 3 illustrates a classification scheme from (International Commission of Snow and Ice, 1981). The scheme suggests that all types of snow avalanches can be composed into three different zones, however, for some avalanche types (e.g. loose snow avalanches) zones can be difficult to differentiate.*

RC18: paragraphs 95 - 100: this section reads well but would benefit from some references to microwave scattering in undisturbed snow as well as avalanche debris.

AC18: There is a large number of publications of various quality study the interaction of microwaves with snow under different conditions. Instead of picking publications describing specific models for microwave scattering at rough surfaces, we think the best approach is similar to (Eckerstorfer and Malnes, 2015) and to provide a general, qualitative description of scattering physics: *Currently, there exists no specific model tailored to the backscatter properties of snow avalanches (cf. (Eckerstorfer and Malnes, 2015, Sect. 5.3)), however, general scattering physics from bi-continuous media and rough surfaces can be applied. In that sense, scattering in snow increases with the spatial correlation length of ice grains (Wiesmann et al., 1998) and also with increased surface- and interface roughness and with decreasing incidence angle θ (Leader, 1971; Fung and Eom, 1982; Kendra et al., 1998).*

RC19: paragraph 105: this section reads like discussion. You have not done your analysis yet but conclude already which parts of an avalanche are detectable and why. if you leave this here, you have to refer to work that tried to assess this at least qualitatively (eg Eckerstorfer et al 2015).

AC19: We agree (See also comment above). Basically, we encounter the same problem as stated in (Eckerstorfer and Malnes, 2015): "To date, no appropriate electromagnetic backscatter model for disturbed snowpacks like avalanche debris exists. Due to this lack of an appropriate model (...) we cannot give an exact theoretical or statistical explanation.". We agree and I think that such an appropriate model is neither required nor of particular help because for avalanches the general scattering physics of rough surfaces should apply and explain already qualitatively the observed scattering behavoir. Still, as we follow similar ideas it makes a lot of sense to cite (Eckerstorfer and Malnes, 2015, Sect 5.3).

RC20: line 131: was manual identification done only in TSX data?

AC20: We will add to section 4.3 *From the images (TSX and S1) avalanche outlines were drawn manually.* (Note, that the single-image section you are referring to will be removed).

RC21: line 180: why do you use 4 db as a threshold? is that based on literature or on your data?

AC21: We will add: *The threshold was determined empirically based on TSX data but other authors also used thresholds of 4–6 dB (Eckerstorfer et al., 2019; Karbou et al., 2018; Vickers et al., 2016).*

RC22: paragraphs 185 - 200: I would consider these paragraphs also as method. please consider moving it there.

AC22: We will add a method-subsection: *"comparison between mapping results".*

RC22.1: and for clarification: how do you deal with the following situation: dataset A shows 2 separate avalanches which are overlapped by 1 avalanche in dataset B?

RC22.1: The problem over overlapping avalanches will be detailed in the above mentioned subsection. The problem is also already discussed in the discussion section 6.6 "avalanche differentiation".

RC23: Figure 6: I am wondering if the readability could be improved by only showing the manually drawn outline, but delete the red lines inside?

AC23: In general, see **AC6** (figures without hashed lines are shown in Fig. 4). This specific figure will be removed anyway (see also **RC8.1** and **RC24**).

RC24: section 5.3: I am unsure why this exercise of comparing detection in single images and change detection images is of interest? I think it is well established that change detection is the only feasible way to reduce uncertainty in satellite avalanche detection.

AC24: See general comment **RC8.1** (will be removed). Instead we provide a few references at the begin of the method section 4.3 and reasons why change detection is the preferred way: *Although well visible avalanches could be manually detected in single radar images, single images are difficult to analyze with automatic methods. As radar systems carry their own illumination system the backscatter signal is primarily determined by topography and land cover type. It is therefore common practise to analyze temporal backscatter variations to separate sudden changes from signals of stable topographic and land cover features (Wiesmann et al., 2001; Eckerstorfer and Malnes, 2015).*

RC25: sections 5.4 and 5.5: this is a very interesting exercise that establishes the upper detection limit of SAR data. Could you consider giving some more details here, about how avalanche size plays into detectability?

AC25: Thanks for this comment. Though lengthening the manuscript, *we will add a new section (5.8) presenting the systematic analysis of detected avalanche sizes.* We found this analysis very interesting and important. See attached figure.

We will add to Sect. 5.4: *We did not found significant differences in area for the lower detection limits: for both, TSX and SPOT-6 the smallest detectable avalanches had an area of 500 m^2. (reference to new Sect. 5.8).*

We will add to Sect. 5.5: *We found that the smallest avalanches detected by S1 have an area of around 2000 m^2 (reference to new Sect. 5.8).*

RC26: section 5.6: that composite is great, very impressive. just to clarify: you did manual detections in entire Switzerland and found 7361 avalanches?

AC26: Yes! But I only counted them systematically using screen-fitting boxes of 12x12 km (1200x1200 px) which was pretty fast (a bit more than 4 hours). We will add: we *manually* counted 7361 avalanches *but did not draw any polygons.*

RC27: line 290: the POD and FNR are calculated for the red or blue box in your study area? same question also when you compare manual detections.

AC27: POD and FNR were calculated for *the entire study area (red polygon in Fig. 1).*, not only for the blue visualization window. We will add this information to figure captions and the text.

RC28: line 290: is the comparison pixel or also feature based? if feature based, how did you handle that for example the automatic detection algorithm split up an avalanche into two features and the manual detection indicates one avalanche?

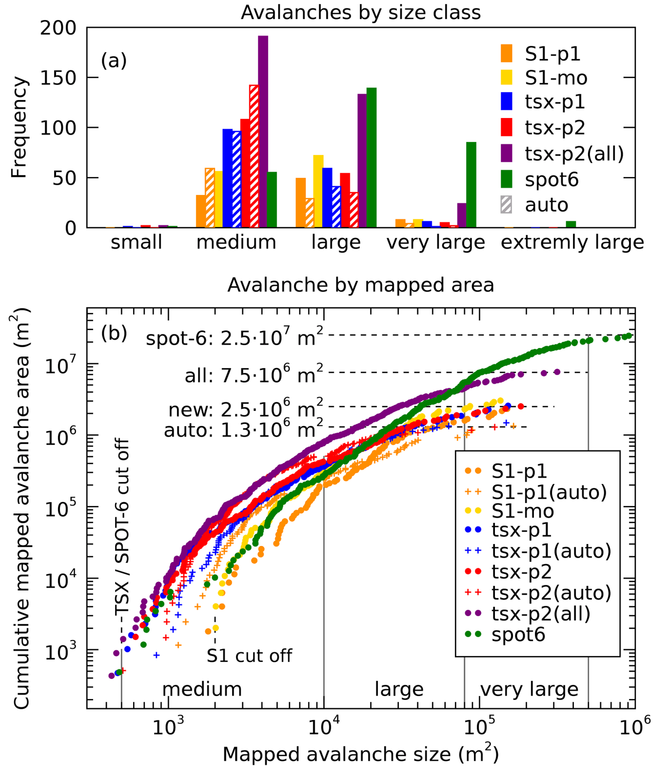

Figure 1. (a): Classification of avalanche area into size classes. (b): the cumulative avalanche area plotted over avalanche size reveals that the smallest avalanches detected by TSX and SPOT-6 is about 500 m^2 and 2000 m^2 for S1. It may surprise that in the study region the total avalanche area of SPOT-6 is an order of magnitude(!) larger than the total area of radar-detected *new* avalanches. Still, a factor of three remains when comparing the area of all (*new, old, unsure*) radar detected avalanches with SPOT-6 (no age classification, only 24% of outlines clearly visible; 76% of avalanches outlines were estimated from partially visible avalanche patches (Bühler et al., 2019)). Considering that with radar mainly the deposition zone has been detected and mapped this difference is reasonable.

AC28: The comparison is feature based. See first result section (line 185-196). This section will be moved to the method (**RC22**). See also discussion 6.6 and **RC22**.

RC29: line 335: these statements read confusing. you have mapped an almost similar number in TSX and Spot-6 images, however, only 68% and 44% of the detected avalanches overlap respectively? Could you explain this a little bit better please!

Also, did the same person outline the avalanches in all data?

AC29: See also **RC22, RC28**. We suggest to add to the results section "SPOT-6 vs. TSX comparison": *Avalanche were mapped independently by E. Hafner in SPOT-6 images (Bühler et al., 2019) and by the second author of this work in TSX* *images. The polygons differed significantly, however, most likely because different features (avalanche origin, path, deposition zone) are visible in optical and radar images. Therefore we decided for a feature-based comparison, i.e. overlapping polygon are considered as avalanches detected in both data sets. Avalanches split up into discontiguous polygons were counted separately, also if all polygons overlap with one single large polygon in the other data set (see also new Sect. 4.7 ->**RC22**).* We hope, that explaining the reason of split up avalanches solves this confusion. The difference 68% vs. 44% is also explained by the differentiability of adjacent avalanches in the succeeding paragraph (339-342).

RC30: section 6.3: this is a very important section in my view. could you say a little bit more about the size distribution of the avalanches and what the cut-off size is for avalanches not detectable in S1, but clearly visible in TSX.

AC30: Based on the added size distribution we suggest to add (in the sense of **RC25**): *The size of smallest detectable avalanches for TSX are "medium" avalanches (500 – 10 000 m^2) with a width of more than 20 m. S1 misses mainly "medium" avalanches smaller than 2 000 m^2. Similar results for S1 with a minimum cutoff of 4 000 m^2 were found by Eckerstorfer et al. (2019).*

RC31: section 6.4: I feel like this is more a repetition of your methods than a discussion of the results. I agree that manual interpretability was improved by all the filtering and smoothing done. however, I somewhat question the use and need of these multiorbital composites, except for visual respresentation of an avalanche cycle. I cannot discern when all these visible avalanches released and which one came first in case of overlapping avalanche activity. this rather long section does not really add much to the overall good discussion of the results.

AC31: We will carefully check this section to decide what should be shortened (*NL mean discussion*) or moved to the method part (*some resolution discussion will be (re)moved to the method section*). But we think especially the multiorbit-composites requires a detailed discussion as it contains may promising approaches and outlooks. See also **RC8.2**.

For discern which avalanche came first, see suggested changes in **RC8.2**.

RC32: section 6.5: the 4 dB threshold might be probematic and could maybe be replaced with more dynamic thresholding considering backscatter intensity change in individual change detection pairs.

AC32: We will add this suggestions. *A dynamic threshold based on backscatter changes in individual image pairs could improve these results (Eckerstorfer et al., 2019).*

RC33: section 6.6: I am somewhat confused that you write about 'avalanche differentiation' but I think you are discussing the detectability of avalanches in each of the data!?

AC33: Detectability and differentiation differ in the following sense: one method could better detect weakly visible large avalanches than another method. or: one method could better differentiate a large patch into multiple smaller avalanches. We mean the latter: *some methods show a much higher potential to differentiate large connected avalanche patches into multiple smaller ones. The reciprocal, two-way comparison of avalanches found in two data sets allows to estimate which of the methods can better differentiate adjacent avalanches.* .

References

Bühler, Y., Hafner, E. D., Zweifel, B., Zesiger, M., and Heisig, H.: Where are the avalanches? Rapid SPOT6 satellite data acquisition to map an extreme avalanche period over the Swiss Alps, The Cryosphere, 13, 3225–3238, https://doi.org/10.5194/tc-13-3225-2019, 2019.

Eckerstorfer, M. and Malnes, E.: Manual detection of snow avalanche debris using high-resolution Radarsat-2 SAR images, Cold Regions Science and Technology, 120, 205 – 218, https://doi.org/10.1016/j.coldregions.2015.08.016, http://www.sciencedirect.com/science/article/pii/S0165232X15002037, 2015.

Eckerstorfer, M., Vickers, H., Malnes, E., and Grahn, J.: Near-Real Time Automatic Snow Avalanche Activity Monitoring System Using Sentinel-1 SAR Data in Norway, Remote Sensing, 11, https://doi.org/10.3390/rs11232863, 2019.

ESA: Sentinel-1: ESA's Radar Observatory Mission for GMES Operational Services (ESA SP-1322/1, March 2012), Tech. rep., ESA, 2012.

Fung, A. K. and Eom, H. J.: Application of a Combined Rough Surface And Volume Scattering Theory to Sea Ice And Snow Backscatter, IEEE Transactions on Geoscience and Remote Sensing, GE-20, 528–536, 1982.

International Commission of Snow and Ice: Avalanche atlas: illustrated international avalanche classification, Unesco Paris, https://unesdoc.unesco.org/ark:/48223/pf0000048004, 1981.

Karbou, F., Coléou, C., Lefort, M., Deschatres, M., Eckert, N., Martin, R., Charvet, G., and Dufour, A.: Monitoring avalanche debris in the French mountains using SAR observations from Sentinel-1 satellites, in: Proceedings of the International Snow Science Workshop, 1, pp. 344–347, 2018.

Kendra, J. R., Sarabandi, K., and Ulaby, F. T.: Radar measurements of snow: experiment and analysis, IEEE Transactions on Geoscience and Remote Sensing, 36, 864–879, 1998.

Leader, J.: The relationship between the Kirchhoff approach and small perturbation analysis in rough surface scattering theory, IEEE Transactions on Antennas and Propagation, 19, 786–788, 1971.

Schweizer, J., Jamieson, J. B., and Skjonsberg, D.: Avalanche forecasting for transportation corridor and backcountry in Glacier National Park (BC, Canada), 25 Years of Snow Avalanche Research, Voss, Norway, 12-16 May 1998, pp. 238–243, 1998.

Schweizer, J., Kronholm, K., and Wiesinger, T.: Verification of regional snowpack stability and avalanche danger, Cold Regions Science and Technology, 37, 277 – 288, https://doi.org/https://doi.org/10.1016/S0165-232X(03)00070-3, http://www.sciencedirect.com/science/article/pii/S0165232X03000703, iSSW 2002: International Snow Science Workshop, 2003.

Small, D.: SAR backscatter multitemporal compositing via local resolution weighting, in: 2012 IEEE International Geoscience and Remote Sensing Symposium, pp. 4521–4524, https://doi.org/10.1109/IGARSS.2012.6350465, 2012.

Vickers, H., Eckerstorfer, M., Malnes, E., Larsen, Y., and Hindberg, H.: A method for automated snow avalanche debris detection through use of synthetic aperture radar (SAR) imaging, Earth and Space Science, 3, 446–462, https://doi.org/10.1002/2016EA000168, 2016.

Wiesmann, A., Mätzler, C., and Weise, T.: Radiometric and structural measurements of snow samples, Radio Science, 33, 273–289, https://doi.org/10.1029/97RS02746, https://agupubs.onlinelibrary.wiley.com/doi/abs/10.1029/97RS02746, 1998.

Wiesmann, A., Wegmuller, U., Honikel, M., Strozzi, T., and Werner, C. L.: Potential and methodology of satellite based SAR for hazard mapping, in: IGARSS 2001. Scanning the Present and Resolving the Future. Proceedings. IEEE 2001 International Geoscience and Remote Sensing Symposium (Cat. No.01CH37217), vol. 7, pp. 3262–3264 vol.7, 2001.

Snow Avalanche Detection and Mapping in multitemporal and multiorbital Radar Images from TerraSAR-X and Sentinel-1

Silvan Leinss[*1], **Raphael Wicki**[*1], **Sämi Holenstein**[1], **Simone Baffelli**[1], **and Yves Bühler**[2]

[*]These authors contribute equally to the paper
[1]Institute of Environmental Engineering, ETH Zurich, Zurich, Switzerland
[2]WSL-Institute for Snow and Avalanche Research SLF, Davos Dorf, Switzerland

Correspondence: Silvan Leinss (leinss@ifu.baug.ethz.ch)

Abstract. Snow avalanches can endanger people and infrastructure, especially in densely populated mountainous regions. In Switzerland, the public is informed by an avalanche bulletin issued twice a day during winter which is based on weather information and snow and avalanches reports from a network of observers. During bad weather, however, information about occurred avalanches can be scarce or even be missing completely. To asses the potential of weather independent radar satellites we compared manual and automatic change detection avalanche mapping results from high resolution TerraSAR-X (TSX) stripmap images and ~~from~~ medium resolution Sentinel-1 (S1) interferometric wide swath images ~~. Within a selected test site in the central Swiss Alps the~~ for a study site in central Switzerland. The TSX results were also compared to available mapping results from high-resolution SPOT-6 optical satellite images. We found that avalanche outlines from TSX and S1 agree well with each other~~but with TSX about 40% more, mainly smaller avalanches were detected. However,~~ . Cut-off thresholds of mapped avalanche areas of 500 m^2 for TSX and 2000 m^2 for S1 were found. S1 provides a much higher spatial and temporal coverage and allows for mapping of the entire Alps at least every 6 days with freely available acquisitions. With costly SPOT-6 images the Alps can be even covered in a single day at meter-resolution, at least for clear sky conditions. For the SPOT-6 and TSX mapping results we found a fair agreement but the temporal information from radar change detection allows for a better separation of overlapping avalanches. Still ~~,~~ the total mapped avalanche area differed by at least a factor of three because with radar, mainly the avalanche deposition zone was detected, whereas the release zone was well visible already in SPOT-6 data. With automatic avalanche mapping we detected around 70 % of ~~the~~ manually mapped new avalanches~~in the same image pair~~, at least when the number of old avalanches is low. To further improve the radar mapping capabilities, we combined S1 images from multiple orbits and polarizations and obtained a notable enhancement of resolution and speckle reduction such that the obtained mapping results are almost comparable to the single orbit TSX change detection results. In a multiorbital S1 ~~moasic~~ mosaic covering entire Switzerland, we ~~detected~~ manually counted 7361 new avalanches which occurred during an extreme avalanche period around Jan 4[th] 2018.

---

1 Introduction

Snow avalanches frequently threaten people and infrastructure in Switzerland and other mountainous countries. Every winter, dozens of people caught in avalanches suffer serious injuries or even die (Techel et al., 2016) and roads and railways have to be closed during periods of high avalanche danger. To inform about the current avalanche danger levels, ranging from 1 (low) to 5 (very high) on the European Avalanche Hazard Scale (Meister, 1995), the WSL-Institute for Snow and Avalanche Research (SLF) publishes an avalanche bulletin twice a day during winter (SLF, 2018e). The bulletin is written by avalanche experts which analyze weather station data, local snow conditions, detailed weather forecast information and avalanche occurrence reported by a network of in-situ observers. Unfortunately ~~, low visibility due to heavy snow fall and~~ during high avalanche activity low visibility and closed valleys and ski resorts ~~closed due to high avalanche activity~~ can lead to incomplete or missing avalanche occurrence information. In such situations, as happened in Switzerland in January 2018 and 2019, avalanches can be mapped manually in optical airborne images (Bühler et al., 2009; Eckerstorfer et al., 2016; Korzeniowska et al., 2017) or satellite images which have to be tasked in rapid mapping mode (Scott, 2009; Lato et al., 2012; Bühler et al., 2019). The resulting avalanche outlines can then be used to update avalanche databases which are of great value for hazard mapping and mitigation measure planning (Rudolf-Miklau et al., 2014). As manual mapping is very time-consuming, attempts have been made to automatize avalanche mapping in optical data (Bühler et al., 2009; Lato et al., 2012; Frauenfelder et al., 2015; Korzeniowska et al., 2017). To provide weather-independent observations the project Alpine Avalanche Forecast service (AAF) evaluated terrestrial and spaceborne radar images (Bühler et al., 2014). They concluded that medium to large avalanche events could be mapped using very high resolution radar satellites but with the drawbacks of limited availability and high costs. Nevertheless, for freely available but medium-resolution Sentinel-1 radar images few but promising manual and automatic avalanche mapping studies exist ~~(Vickers et al., 2016; Eckerstorfer et al., 2017; Wesselink et al., 2017; Abermann et al., 2019)~~ (Vickers et al., 2016; Eckerstorfer et al., 2017; Wesselink et al., 2017; Abermann et al., 2019; Eckerstorfer et al., 2019) .

To evaluate the applicability of high and medium resolution radar images for avalanche detection in the Swiss Alps we compare 10-meter resolution Sentinel-1 radar images, 3-meter resolution TerraSAR-X radar images, and 1.5 meter resolution SPOT-6 optical images ~~with each other~~ and analyze different methods ~~to detect avalanches from single,~~ using multitemporal and multiorbital radar images for two extreme avalanche events which occurred in Switzerland in Jan 2018.

2 Study area and data

The study area, shown in Fig. 1, was determined by the spatial and temporal availability of high resolution radar images from the satellite TerraSAR-X (TSX), operated by the German Aerospace Center (DLR). No systematic TSX coverage is available ~~because TSX acquires data upon request for scientists and private customers~~ over Switzerland because data are acquired upon request (Werninghaus and Buckreuss, 2010). To cover the two extreme avalanche events around Jan 4th and 22nd 2018 (Fig. 2) with images acquired from identical orbits as good as possible we searched the ~~TSX~~ archive for a sequence of images which limited the study area to the Alps of Uri in central Switzerland. The orbit repeat time defines the dates and limits the revisit time to 11 days for the first event and 22 days for the second one (one acquisition missing). The images were acquired

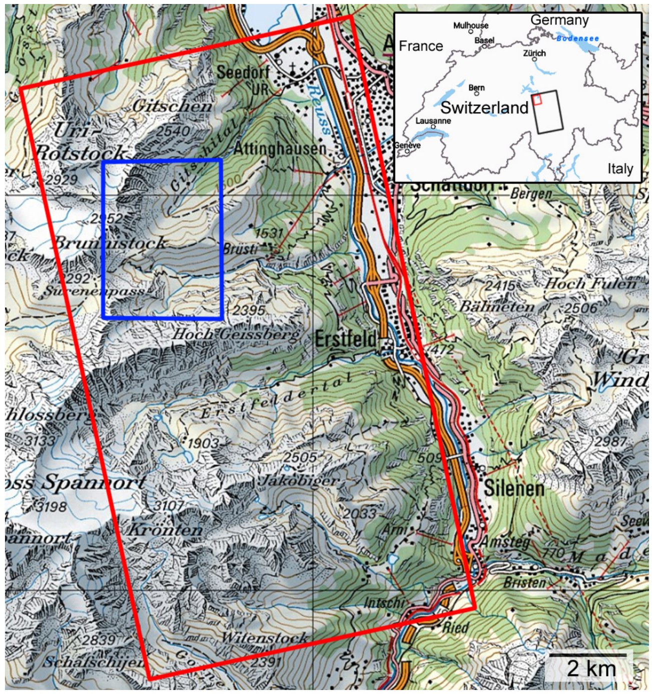

Figure 1. Area selected for avalanche mapping (Red rectangle). Blue rectangle: subset used to visualize radar images and mapping results (46°51′N, 8°34′E). The black rectangle in the insets shows the ~~full~~ footprint of the full TSX scene over Switzerland ~~(black rectangle)~~. © 2019 swisstopo (JD100042), reproduced with the authorisation of swisstopo (JA100120).

Table 1. Satellite data with local acquisition time (CET = UTC+1). ~~The TSX~~ Acquisition modes are abbreviated as SM (stripmap), IW (interferometric wide swath), and MS (single pass multi-strip collection). The full list of S1 ~~images were acquired looking east from ascending orbits~~ acquisitions used for the composite of Switzerland is listed in Table A1.

	satellite	~~Date, local time~~ date, time (CET)	mode	pol. / band
	TSX	2017-12-31 ~~-~~ 18:09	SM	HH
	TSX	2018-01-11 ~~-~~ 18:09	SM	HH
~~Satellite~~	TSX	2018-02-02 ~~-~~ 18:09	SM	HH
	S1	2017-12-31 ~~-~~ 18:14	~~IW-1~~ IW-1	VV~~/~~, VH
	S1	2018-01-12 ~~-~~ 18:14	~~IW-1~~ IW-1	VV~~/~~, VH
	SPOT-6	2018-01-24 ~~-~~ 10:03	MS	R,G,B,NIR

in X-band (9.6 GHz) with the standard TSX stripmap mode (SM) at a nominal single-look complex (slc) resolution of 2.3×3.3 m (rg×az). Acquisitions are listed in Table 1. Snow and weather conditions during the two avalanche events are summarized by Bühler et al. (2019). Details are provided by Winkler et al. (2019) and SLF (2018a, b, c, d) (in German).

The full TSX scene (black rectangle in the inset in Fig. 1) covers 55×35 km^2 but for the analysis we selected an area of 15.3×8.6 km^2 ~~which shows a very high avalanche activity~~ (red rectangle in Fig. 1) ~~. The altitude of the~~

~~selected area~~ where both the TSX and the validation data (Bühler et al., 2019) show a very high avalanche activity. The selected area contains steep topography which ranges from 400 - 3200 m.a.s.l.. For visualization of results we show in the following only a small subset ~~of the selected area (~~ (blue rectangle in Fig. 1~~, blue rectangle)~~) of the analyzed area.

Radar images of the satellite Sentinel-1 (S1) were analyzed for comparison. S1 images are acquired globally and systematically and are free and openly available for download within 24 hours after acquisition ~~(Davidson et al., 2010)~~ (ESA, 2012). Currently, S1 consists of two satellites, S1-A and S1-B, which alternately image central Europe every six days from the same orbit with ~~a~~ an slc resolution of 2.7×22.5 m (rg×az) ~~with~~ in the interferometric wide swath mode (IW). The S1 images, covering $250 \times 170\,\mathrm{km}^2$, were selected such that they had orbits and acquisition times similar to TSX.

The first analyzed images of both satellites were acquired on 2017-12-31 a few minutes after 18 h local time (Table 1). The second TSX image was acquired on 2018-01-11, one day before the second S1 image (2018-01-12). On the day in between, the avalanche activity was very low (Fig. 2) and ~~the avalanche danger level was moderate for the selected area. Meteorological~~ meteorological conditions were relatively stable (SLF, 2018b).

To assess avalanche detection of entire Switzerland, S1 acquisitions were carefully selected from multiple orbits during a 5 day period from before and after the first event (Gray shading in Fig. 2, acquisition details in Table A1).

To analyze the second avalanche event, the SLF ordered optical SPOT-6 images ~~which were~~ acquired with the single-pass multi-strip collection mode~~through which~~ . With this mode the most of the Swiss alps ($300 \times 40\,\mathrm{km}^2$) could be imaged in a single day (2018-01-24), at a resolution of 1.5 m. These images were visually searched for avalanches by an expert (Bühler et al., 2019). For comparison we also analyzed TSX data from 2018-02-02, acquired 9 days later.

2.1 ~~Avalanche events and meteorological conditions~~

~~January 2018 was exceptionally warm, humid and stormy. It was the warmest January recorded by systematic measurements since 1864 and many stations reported record sums for new snow and precipitation (MeteoSchweiz, 2018) .~~

~~On Jan , embedded in warm and humid winds from the Atlantic Ocean, with a snow line above , the storm "Burglind" hit Switzerland and wind speeds up to were measured on alpine summits. Humid Mediterranean currents followed the storm. During the first avalanche period from Jan 3–, the avalanche danger level was generally 3 (considerable) but raised to 4 (high) on Jan 4/, and on the for a major part of the Swiss alps (SLF, 2018a). During sunny days from Jan 13–the snow line raised up to followed by almost daily precipitation and strong winds from north-west~~

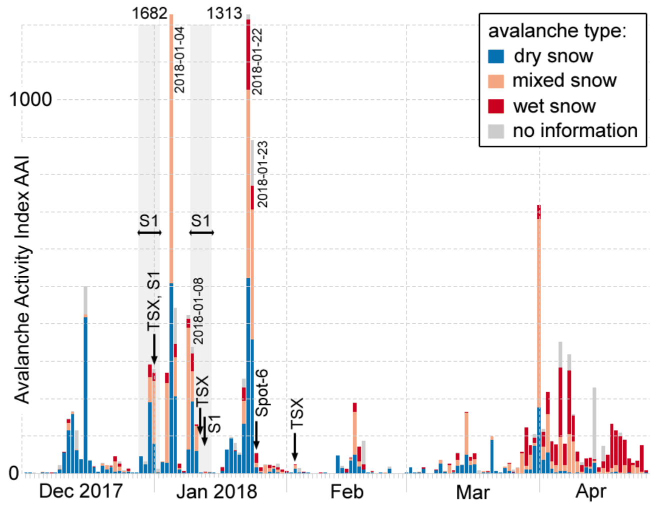

Figure 2. ~~Avalanche Activity Index~~ The avalanche activity index is the weighted sum of all reported avalanches for Switzerland ~~modified after Winkler et al. (2019)~~(Schweizer et al., 2003, 1998). Dry snow avalanches which started high up but were slowed down at medium altitude by wet snow are indicated as "mixed snow" in the legend. Satellite acquisitions dates are indicated by arrows. Images for the multiorbital S1 composite were acquired during the gray shaded periods (see also Table A1). Figure modified after Winkler et al. (2019).

~~on Jan 16–. Wind speeds of over occurred during the storms "Evi" and "Friedericke" on Jan and . On Jan 20/extreme snowfall was registered. From Jan 21–, the avalanche activity reached a new three-day record for the past 19 years since the avalanche winter in 1999 (Winkler et al., 2019). Due to the extraordinary avalanche situation, the avalanche danger level was raised to 5 (very high) on Jan 21/(SLF, 2018c). After Jan the situation eased and temperatures were very warm with a snowline rising from to over until end of January. The avalanche activity was low and the avalanche danger level was mainly moderate for the analyzed area. On Feb temperature dropped and around of snow fell (SLF, 2018d) . Therefore, snow conditions were slightly different between the TSX and SPOT-6 data but only a few new avalanches occurred (Fig. 2).~~

3 Radar backscatter physics of avalanches

We detected avalanches based on the radar backscatter signal and their visual appearance (shape). ~~As illustrated in~~ Fig. 3 ~~, all types of snow avalanches are composed by~~ illustrates a classification scheme from (International Commission of Snow and Ice, 1981) . The scheme suggests that all avalanche types are composed of three different zones ~~(International Commission of Snow and Ice, 1981).~~ but for some avalanche types (e.g. loose snow avalanches)

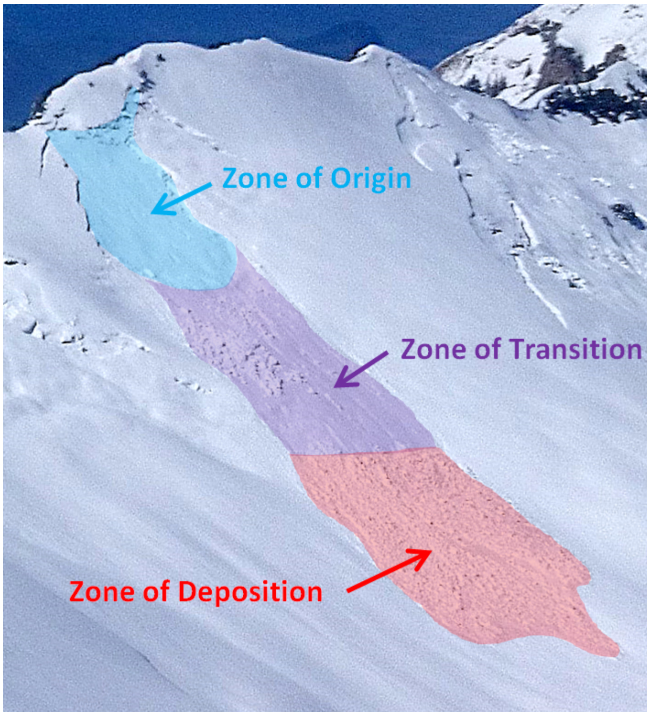

Figure 3. Different avalanche zones illustrated by a slab avalanche.

zones can be difficult to differentiate. The most upslope part is the release area (Fig. 3, blue) with a smooth surface caused by the failure of the weak layer, followed by the zone of transition (purple) with the stauchwall and some deposition caused by the terrain roughness, and finally the tongue-shaped zone of deposition (red) at the bottom which is covered by densely compacted snow granules.

Based on snow properties, the different zones show a different radar backscatter signal. In first order scattering physics the total backscatter intensity of a snow pack, σ^0_{snow}, can be composed ~~by~~ of scattering from the snow surface, σ^0_{surf}, scattering from the snow volume, σ^0_{vol}, scattering from the ground below the snow pack, $\sigma^0_{\mathrm{ground}}$, and scattering from higher order interactions between different structures in the snow pack $\sigma^0_{\mathrm{inter}}$. ~~Generally, scattering depends on the~~ Currently, there exists no specific model tailored to the backscatter properties of snow avalanches (cf. Eckerstorfer and Malnes, 2015, Sect. 5.3), however, general scattering physics from bi-continuous media and rough surfaces can be applied. In that sense, scattering in snow increases with the spatial correlation length of ice grains (Wiesmann et al., 1998) and also with increased surface- and interface roughness and ~~on the~~ with decreasing incidence angle θ (Leader, 1971; Fung and Eom, 1982; Kendra et al., 1998).

$$\sigma^0_{\mathrm{snow}}(\theta) = \sigma^0_{\mathrm{surf}}(\theta) + \sigma^0_{\mathrm{vol}}(\theta) + \sigma^0_{\mathrm{ground}}(\theta) + \sigma^0_{\mathrm{inter.}}(\theta) \quad (1)$$

For plain dry snow of few meters depth scattering at the ground usually dominates the signal because microwaves between 1 and 10 GHz are weakly scattered at the snow surface and within the snow volume and penetrate therefore the snow pack to the ground ~~. There,~~ (Xu et al., 2012; Cumming, 1952; Rignot et al., 2001), see also conclusion and simulations in Leinss et al. (2015). For dry snow the ground roughness determines the backscatter signal but for smooth ground mainly forward scattering (away from the sensor) occurs. For deeper snow ~~volume scattering can dominate the signal~~ or higher frequencies the signal can be dominated by volume scattering (Watte and MacDonald, 1970).

In contrast to plain dry snow, snow is deeper and denser in the deposition zone ~~and the surface is rougher. Due~~ where the surfaces of the avalanche debris can be very rough. Because of the higher dielectric contrast due to the higher permittivity (Matzler, 1996), the contribution of σ^0_{vol} and σ^0_{surf} to the total backscatter intensity increases. ~~Both ,~~ Both the rough surface and the ~~volume scatters~~ debris volume scatter radiation more omnidirectional (diffuse scattering) compared to an undisturbed snow pack over smooth ground (specular scattering).

For plain wet snow, however, the incoming radar waves are weakly ~~scattered back~~ backscattered at the air-snow interface ~~whereas~~ because most radiation is lost by absorption ~~and forward scattering~~(Tiuri et al., 1984; Cumming, 1952) and also by forward scattering described by Fresnel coefficients.

As the volume and ground contribution is negligible for wet snow avalanche debris, the dominant backscatter signal results from omnidirectional scattering at the increased surface roughness in the deposition zone of avalanches ~~.~~ (cf. Eckerstorfer and Malnes, 2015, Sect. 5.3).

~~In radar images~~Based on the above scattering physics, the zone of origin is very difficult to detect ~~because only~~ in radar images because the weakly scattering snow volume is reduced without major changes in the surface roughness. The zone of transition ~~is~~ should be only sometimes visible, depending on the deposition of avalanche debris. Therefore, mostly the deposition zone can be detected by a brighter backscatter signal and the mostly elongated, tongue shaped geometry.

To obtain a high backscatter contrast with respect to the avalanche surrounding the local incidence angle θ should be far away from zero ~~to avoid~~ (i.e. away from layover) to avoid the intense specular backreflection from smooth surfaces. Therefore, the visibility of avalanches in radar images should be much better for slopes facing off the radar. These slopes are ~~anyway~~ also imaged with a higher ground-range resolution $\delta_{\mathrm{sr}}/\cos\theta$ which can be close to the slant-range resolution δ_{sr}.

4 Methods

4.1 Data preprocessing

All radar products were downloaded in the single look complex (SLC) format. The data were preprocessed with the ESA SNAP Sentinel-1 toolbox and also with the GAMMA software for comparison. The workflow using GAMMA was implemented with Nextflow (Di Tommaso et al., 2017) to speed up execution and code development and to ensure a reproducible analysis. Preprocessing consists of coregistration, multilooking for reduction of radar speckle (TSX: 6×5 px, S1: 4×1 px), orthorectification, and generation of radar shadow and layover masks. The SNAP workflow for S1 images is shown in Fig. A1. We did not apply any radiometric terrain correction as the visible topography helps to identify the avalanche path direction.

For orthorectification we used the Swiss elevation model SwissAlti3D (2013) downsampled from 2 m to 30 m resolution. We noticed, however, that despite of using the same DEM and output resolution, sharp topographic features seem to be better orthorectified with the GAMMA software which might use a more precise spatial interpolation. The radar images were orthorectified to a resolution of 5x5 m (TSX) and 15x15 m (S1) and the backscatter signal in dB was saved to geotiff files. The exact radiometric normalization is irrelevant, because we did not apply any radiometric terrain correction (Small, 2011) and different ellipsoidal corrections ($\sigma^0_{\mathrm{E}}, \gamma^0_{\mathrm{E}}$) differ only by almost constant factors. Since the TSX data was acquired with a single polarization (the co-polar channel HH) we also used only the co-polar channel (VV) of the two available polarizations of S1 to obtain a fair comparison. For the multiorbital composites, we used both polarizations of S1 (VVand , VH).

4.2 ~~Single image avalanche detection~~

~~For avalanche detection by visual inspection in single images, areas with radar shadow and layover were masked out. The images (as shown in Fig. ??) were then systematically searched for bright features matching the tongue shaped geometry of the avalanche deposition zone. Potential avalanches were manually contoured to create an avalanche mask. For uncertain cases, a topographic relief map was used to decide if the identified shape corresponds to a possible flow path.~~

4.2 Two-image composite avalanche detection

~~Since detection in single images is difficult , we composed two consecutive acquisitions from the same orbit to an RGB change detection image~~Although avalanches could be manually detected in single radar images they are difficult to analyze with automatic methods. As radar systems carry their own illumination system the backscatter signal is primarily determined by topography and land cover type. It is therefore common practise to analyze change detection images to separate sudden backscatter changes from stable topographic and land cover features (Wiesmann et al., 2001; Eckerstorfer and Malnes, 2015). To correct for large-scale backscatter changes due to wet snow a 500 m highpass filter was applied to the backscatter difference between ~~the two~~ two consecutive images. Examples for TSX and S1 are shown in Figs. 4a and 4b. To create the images, the backscatter intensities in dB were normalized by clipping the lower and upper 1%. Consecutive images were then stored in the channels [R, G, B] = [img2, img1, img1] so that backscatter changes are well visible by the red-cyan contrast~~: increased backscatter appears red, decreased backscatter appears light blue (cyan), and unchanged backscatter appears gray.~~ . From the images (TSX and S1) avalanche outlines were drawn manually.

The ~~RGB~~ change detection images ~~allows~~ allow for a temporal classification of avalanches into three classes ~~:~~ (*new*, *old*, *unsure*~~, and *unsure*~~). *New* avalanches appear red because of increased backscattering and are therefore assumed to have occurred between the first and the second acquisition. *Old* avalanches, with a decreasing backscatter signal, appear blue are therefore assumed to have occurred before the first acquisition. Bright features with ~~an~~ unchanged backscatter intensity appear almost white and are classified as *unsure* if they look like avalanches.

~~Multiorbital S1 change detection image as in Fig. 4c but with a non-local mean filter applied. Orthorectified with the swissALTI3D ©2019 swisstopo (JD100042), reproduced with the authorisation of swisstopo (JA100120). The corresponding full scene is shown in Fig. 7 and covers entire Switzerland.~~

4.3 Multiorbital composite image for Switzerland

~~In contrast to the limited availability of TSX data, the~~ The free and systematic availability of S1 radar images and the short revisit period of ~~only six days over central Europe allows~~ six days allow for creation of an RGB composite change detection image covering entire Switzerland. Therefore, 12 images, acquired between 2017-12-28 and 2018-01-01 from different orbits, were combined into an image before the first avalanche event (Jan 4$^{\mathrm{th}}$). Another 12 images, acquired between 2018-01-09 and 2018-01-12 with an identical imaging geometry, were used for the post-avalanche event image. The images (listed in Table A1) were preprocessed according to Sect. 4.1. To reduce radar speckle we averaged both polarizations and weighted the cross-pol channel (VH) by the ratio a of the co- and cross-pol backscatter intensities averaged over the ~~entire scene~~acquisition footprint:

$$S = \frac{S_{\mathrm{VV}} + a\,S_{\mathrm{VH}}}{1+a} \qquad \text{with} \qquad a = \frac{\langle S_{\mathrm{VV}}\rangle}{\langle S_{\mathrm{VH}}\rangle} \tag{2}$$

Then, the weighted mean was converted to dB and scenes from different ascending and descending orbits were aver-

~~Subset of single radar image TSX(01-11).~~

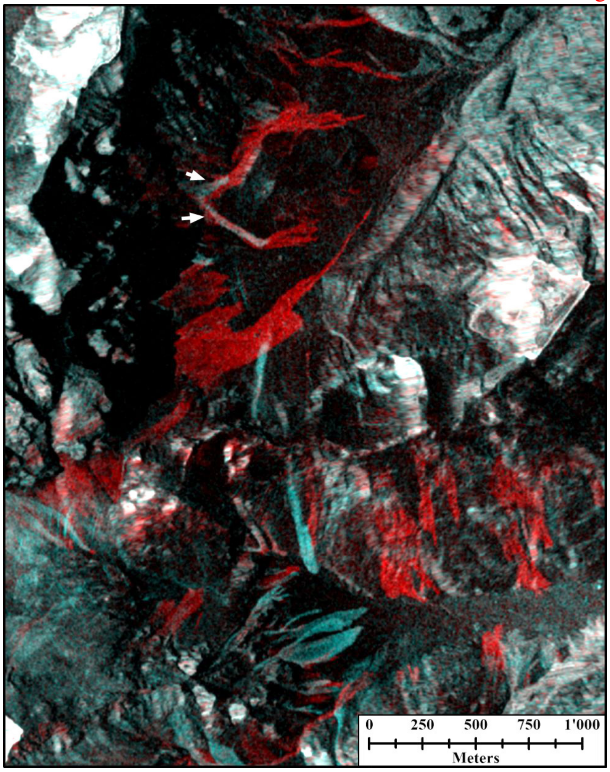

(a) Subset of change detection image tsx(12-31 / 01-11).

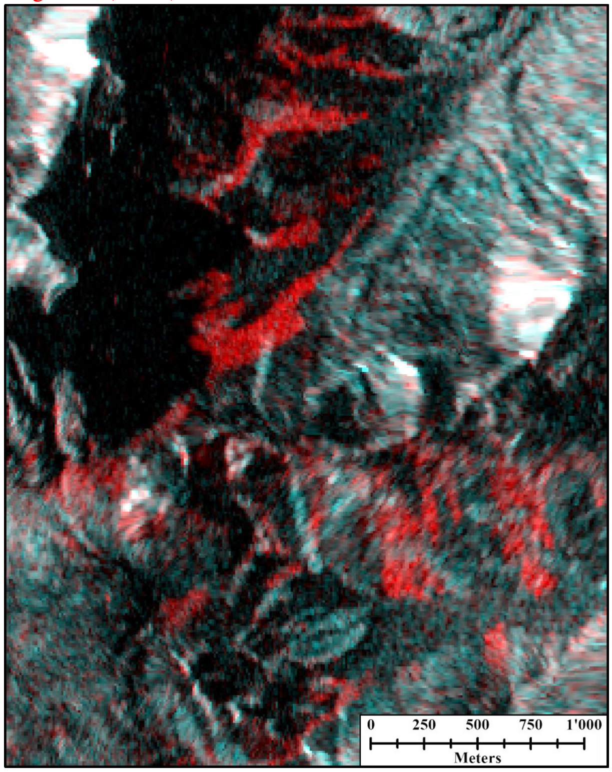

(b) Subset of change detection image S1(12-31 / 01-12).

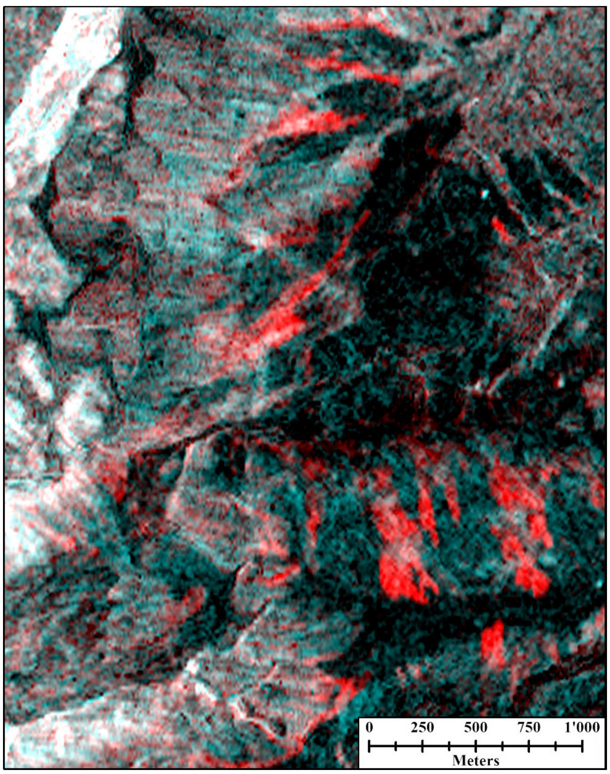

(c) Subset of S1 multiorbital change detection image from the two data sets 2017-12-28 – 2018-01-01 vs. 2018-01-09 – 2018-01-12.

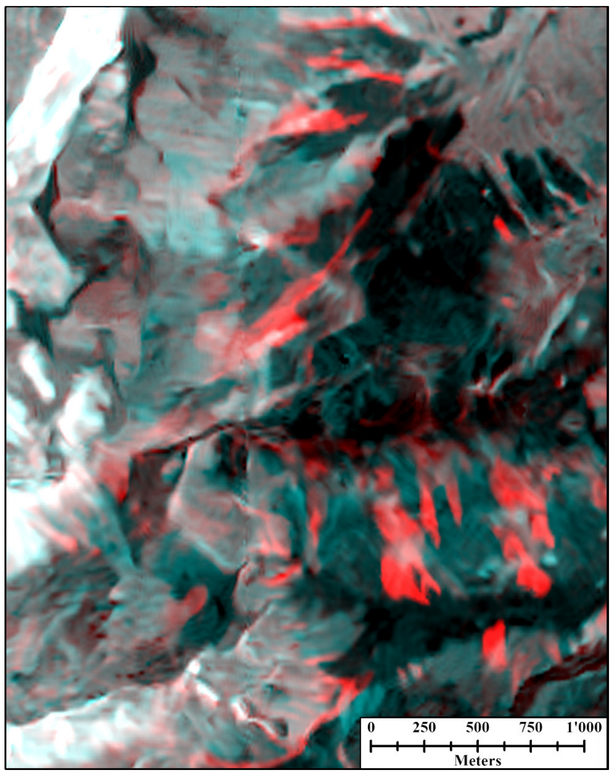

(d) ~~Subsets of the study area:~~ Multiorbital S1 change detection image as in (~~a~~c) ~~single radar image,~~ but with non-local mean filter applied.

Figure 4. (~~b~~a,~~c~~b) TSX and S1 change detection images ~~, and~~ of a subsets of the study area (~~d~~cf. Fig. 1)~~S1 multiorbital composite~~. The radar view direction is ~~always from the~~ ascending (left to right) incidence angles are 29° and 34°. Arrows in (~~b~~a) indicate old avalanches overrun by new ones. (c) S1 multiorbital composite with (d) non-local mean filter applied. All TerraSAR-X and Copernicus Sentinel data (2019) were orthorectified with the swissALTI3D © 2019 swisstopo (JD100042), reproduced with the authorisation of swisstopo (JA100120).

aged~~in overlapping areas~~. Thereby, a relatively homogeneous bright image is generated where layover areas lighten up the relatively dark slopes facing away from the radar without screening too much of the contained details (Fig. 4c). To further reduce noise but to preserve edges in the mosaic images, we applied a non-local mean filter (Jin et al., 2011; Condat, 2010). The filtered image is shown in Fig. 4d.

4.4 Relative brightness of snow avalanches

To analyze the brightness of avalanches relative to their surrounding, we calculated the ratio of the mean backscatter signal of an avalanche area and its surrounding area. Therefore, a ~~visually determined~~ manually generated avalanche mask was dilated once by 9 and once by 18 pixels. The difference of the two masks defines the surrounding. For the avalanche mask, the visual avalanche mask was eroded by 3 pixels to reduce manual contouring errors. To obtain statistically significant results we calculated the backscatter ratios only for avalanches and surrounding areas larger than 100 pixels.

4.5 Automated avalanche detection

As manual avalanche mapping is time consuming, a reliable automation of this process would make the mapping data quickly available for further application. Therefore, different attempts have been made to automatically detect avalanches mainly on the two satellite platforms S1 ~~(Vickers et al., 2016; Wesselink et al., 2017; Abermann et al., 2019)~~ (Vickers et al., 2016; Wesselink et al., 2017; Abermann et al., 2019; Eckerstorfer et al., 2019), and Radarsat-2 (Hamar et al., 2016; Wesselink et al., 2017). The general workflow in these papers is quite similar to ours. All methods are based on two-image change detection, application of various masks (layover, shadow, water bodies, forest), thresholding and filtering of extracted avalanche properties.

In addition to a shadow and layover mask, we applied a slope dependent mask to limit the detection to potential avalanche deposition zones for which we expect the strongest backscatter change. By definition, friction is larger in the deposition zone than the downhill-slope force. Therefore, slopes with an inclination larger than 35°, which typically occur in the zone of origin, are masked out (Bühler et al., 2009).

For noise reduction but to preserve avalanche edges, a 5×5 px median filter was applied to the backscatter difference images in dB. As avalanches should have a well defined edge, an edge mask was generated by applying a Sobel filter with a 5×5 kernel to the median filtered difference image.

In the median filtered difference image, from all pixels brighter than a threshold of 4 dB, the brightest 5% were considered as the mask of potential avalanches. The threshold was determined empirically based on TSX data but other authors also used thresholds of 4–6 dB (Eckerstorfer et al., 2019; Karbou et al., 2018; Vickers et al., 2016). To remove isolated bright pixels from the mask, we determined around each continuous area an ellipse and removed areas with a major axis shorter than 15 pixels (TSX: 45 m, S1:225 m). Additionally, only potential avalanches for which more than 10 pixels intersect with the edge mask were considered for the final avalanche mask.

5 ~~Results~~

4.1 Comparison between mapping results

None of the mapping results obtained from TSX, S1, or SPOT-6 can be considered as real ground truth and different avalanches or avalanche shapes were detected with the different methods and satellites. Also, ambiguous relations can exist when a single large avalanche in one mapping result appears as multiple smaller avalanches in another mapping result. This makes the evaluation of binary classifies (e.g. probability of detection or false discovery rate) difficult or even impossible. We refrained from using a pixel-to-pixel comparison which would have demanded a manual mapping precision on the pixel level which contradicts the subjective mapping by an experienced expert who sometimes estimates an avalanche outline from discontinuous avalanche patches.

As a remedy we compare results from two data sets A and B by reciprocal counting of avalanches which overlap in both data sets (considered as "found") and avalanches which do not overlap (considered as "not found"). These numbers differ depending on the direction in which the comparison is done (A→B or B→A). Depending which data sets is considered as ground truth, avalanches which were "not found" can be either regarded as false negative alarms (missed) or as false positive alarms (false alarm).

For conciseness we ~~refer in the following sections to the two single radar images from 2018-01-11 and 2018-02-02 as TSX(01-11) and TSX(02-02). Similar, we refer to the corresponding TSX~~ abbreviate the RGB change detection images ~~as tsx(12-31~~by acquisition month and day (mm-dd/~~01-11) and tsx(01-11/02-02)and to the S1 change detection image 2017-12-31 vs. 2018-01-12 as S1(12-31/01-12).~~ mm-dd).

4.2 ~~TSX single image~~

~~In the first image TSX(01-11), acquired after the first avalanche event, in total 142 avalanches were detected by visual inspection. Figure ?? shows a subset of the analyzed scene. Some avalanches can be clearly identified by their bright backscatter signal and their tongue-like shape.~~

~~Single TSX backscatter image from 2018-02-02 (after the second avalanche event) including manually masked avalanches. Orthorectified with the swissALTI3D ©2019 swisstopo (JD100042), reproduced with the authorisation of swisstopo (JA100120).~~

Table 2. Number and classification of manually detected avalanches ~~from~~ in TSX ~~change detection~~ images ~~which cover~~ covering the first and the second avalanche period.

change detection image	total	*new*	*unsure*	*old*
tsx(12-31 / 01-11)	267	164	84	19
tsx(01-11 / 02-02)	351	170	146	35

~~Number of manually detected avalanches in TSX single images acquired after the first and after the second avalanche event. TSX image total number of found avalanchesTSX(01-11) 142TSX(02-02) 120~~

~~In the second image, TSX(02-02), acquired after the second avalanche event, a total of 120 avalanches were detected. Figure ?? shows a subset of the analyzed scene with an overlay of the manually generated avalanche mask. For this image, an unambiguous identification of avalanches was difficult. Because of the heavy avalanche activity on Jan 22/, multiple small new avalanches could have formed larger connected areas or even run over the same area multiple times such that the individual avalanches could not be identified. Because 10 days elapsed since the main avalanche event, avalanches progressively lost contrast to the surrounding snow due to loss of the surface roughness by surface melt, windblown snow or fresh snow.~~

5 Results

5.1 TSX change detection

In the change detection image tsx(12-31 / 01-11), covering the first avalanche period, a total of 267 avalanches were manually detected ~~.~~ in the study area (red polygon in Fig. 1). As detailed in Table 2, 164 avalanches were classified as *new* and 19 were classified as *old* avalanches. For 84 avalanches a clear assignment to *new* or *old* was not possible. Therefore, ~~they were assigned~~ we assigned them to the class *unsure*. For example, in the upper part of Fig. 4a ~~,~~ arrows indicate two large new avalanches which completely covered two small old avalanches~~(indicated by arrows)~~. Therefore, ~~the~~ their backscatter signal did not change and these old avalanches were classified as *unsure* (though they could be classified as *old* using spatial context information).

In the change detection image tsx(01-11 / 02-02), covering the second avalanche period, a total of 351 avalanches were detected, composed ~~by~~ of 170 *new* avalanches, 35 *old* ones and 146 *unsure* cases. Most of these *unsure* avalanches were actually classified as *new* after the first avalanche period but overrun by new avalanches during the second avalanche period (compare Fig. A2 with Fig. A3). Therefore, the number of *old* avalanches seems to remains low.

5.2 ~~TSX change detection compared to single images~~

~~The TSX change detection images indicates a significantly enhanced sensitivity to avalanches compared to single TSX images. It seems that about twice as much avalanches (of class *new* and *unsure*) have been detected (248 vs. 142 and 316 vs. 120 avalanches, Table ?? vs. Table 2). However, around 90% of the avalanches detected in the single image overlap with one or more avalanches classified as *new* or *unsure* in the change detection image. The better differentiation into multiple small avalanches is the main reason why the detection numbers in the change detection image are higher.~~

~~As detailed in Table ??a, when counting how many of 142 avalanches from TSX(01-11) overlap with avalanches from tsx(12-31/01-11), we found that 71% (101 avalanches) were also found as *new* and 12 avalanches were not found. Vice versa, 32% (53/164 avalanches) classified as *new* by change detection were not found in the single image (Table ??b).~~

~~A similar result is obtained for the 120 avalanches from the second single image TSX(02-02). As detailed in Table ??c, 85 of 120 avalanches (71%) were also detected as *new* in the change detection image and 6 avalanches were not found. Vice versa, 31% (52/170) of avalanches classified as *new* were not detected in the single image (Table ??d).~~

~~Number of avalanches in single image which correspond to avalanches in TSX change detection image (a, c) and reverse correspondence of *new* avalanches from TSX change detection (b, d).~~

~~(a) total *new unsure old* not found142 101 22 7 12(b) total not found164 53(c) total *new unsure old* not found120 85 27 2 6(d) total not found170 52~~

5.2 TSX compared to optical ~~SPOT-6~~SPOT-6

The SPOT-6 images were acquired immediately after the second avalanche event in the morning of Jan 24th. ~~Unfortunately due~~ Avalanche were mapped by E. Hafner in SPOT-6 images (Bühler et al., 2019). They found that only 24% of outlines were clearly visible; 76% of the avalanches outlines were estimated between partially visible release and deposit areas. In the study area, the SPOT-6 avalanches did not contain any age information but the authors conclude that $20-45\%$ of avalanches were already released many of them are actually old avalanches.

Due to the 11 day revisit time of TSX, the ~~first~~ next available TSX image ~~from after the event~~ was acquired 9 days ~~later~~ after the second event in the evening of Feb 2nd. During this 9 days surface melt occurred followed by about 20 cm of new snow on Feb 1st. Due to changing snow properties the contrast between avalanches and the surrounding snow has very likely decreased.

~~Nevertheless, as detailed in Table 3a, we found that 68% (85/120) of the avalanches detected in TSX(02-02) were also detected in the~~ Without knowledge of the SPOT-6 ~~image. Interestingly, of the remaining third (35/120)the majority (28 avalanches) were located in the east~~

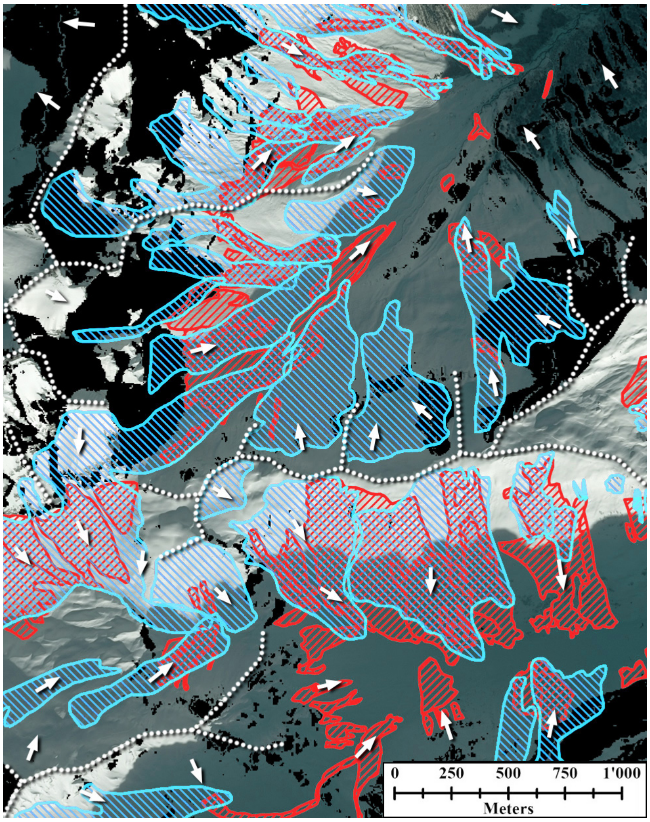

Figure 5. Manually mapped avalanches (blue) from the SPOT-6 image 2018-01-24 (background) vs. change detection results from tsx(01-11 / 02-02) (red, all classes) in a subset of the entire study area (cf. Fig. 1). Orthorectified with the swissALTI3D © 2019 swisstopo (JD100042), reproduced with the authorisation of swisstopo (JA100120). Radar shadow is added in black. Dots show mountain ridges and arrows the down-slope direction.

shadowmapping results, avalanche were mapped in the TSX images independently by the second author of this work. The outlines differed significantly, however, most likely because different features (avalanche origin, path, deposit zone) are visible in optical and radar images. Therefore we decided for a feature-based comparison, i.e. overlapping polygon are considered as detected in both data sets. Avalanches split up into discontinuous polygons were counted separately, even if all polygons overlap with one single large polygon in the other data set (Sect. 4.1).

Similar,

Despite of non-optimal acquisition timing and mapping conditions, Table 3a shows for the change detection image tsx(01-11 / 02-02) Table 3b shows that 68% (215/316) of the avalanches detected as *new* or *unsure* were also detected in the SPOT-6 image. The remaining Interestingly, of the remaining third (101were not detected, again, the majority of them /316) the majority (84 avalanches) were located in the cast shadow.

Table 3. (a) Number of avalanches detected in single (a) and TSX change detection (b) TSX radar images image compared to avalanches which were also detected in the optical SPOT-6 data. (eb): reverse correspondence of avalanches from SPOT-6 to *new* and *unsure* avalanches from the radar change detection image. Avalanches which were not found are grouped depending on if they are located in the cast shadow (a,b) or in the radar shadow (eb).

(a)	of *new/unsure* in tsx(01-11 / 02-02)	→
	total	
	120 85 35 (28 / 7) (b) total found not found(in / not in cast shadow)316	
(eb)	of SPOT-6 (01-24)	
	total	
	286	

Vice versa, 44% (125/286) of the optically detected avalanches were also found in the TSX change detection image (Table 3eb) but more than half of the optically detected avalanches were not found. 20% (57/286) could not be found because they are located in the radar shadow and 36% (104/286) had a too low backscatter contrast to be visible with radar. We did not found significant differences in area for the lower detection limits: for both, TSX and SPOT-6 the smallest detectable avalanches had an area of 500 m^2 (Sect. 5.1).

With Using the temporal information from radar change detection the 125 avalanches detected with SPOT-6 but also with TSX (Table 3eb) can be further classified into 27 *new*, 38 *unsure*, and 6 *old* avalanches. The remaining 54 avalanches could not be uniquely unambiguously classified, because they cover areas which were differentiated into multiple different classes by radar whereas such a temporal classification is difficult with single SPOT6 images (Bühler et al., 2019).

Figure 5 shows a subset of the SPOT-6 images and visualizes the manually mapped avalanches. Especially in the lower part of the image, in the cast shadow, many small radar-detected avalanches (red) were not found in the optical analysis (blue). With radar, avalanches could generally not be detected in the radar shadow or layover (added with black) but also many other avalanche were missed by radar.

5.3 TSX compared to S1 change detection

To asses the added value of high resolution TSX images compared we compared them to medium resolution S1 imageswe compared the corresponding mapping results. Images from . We chose the first avalanche period were chosen to simplify counting because of less overlapping old and new avalanches. In the S1 change detection image S1(12-31 / 01-12) a total of 89 *new*, 13 *unsure*, and 16 *old* avalanches were found. Compared to TSX, the The S1 change detection image shows a significantly lower resolution than TSX (Fig. 4a vs. Fig. 4b) such that

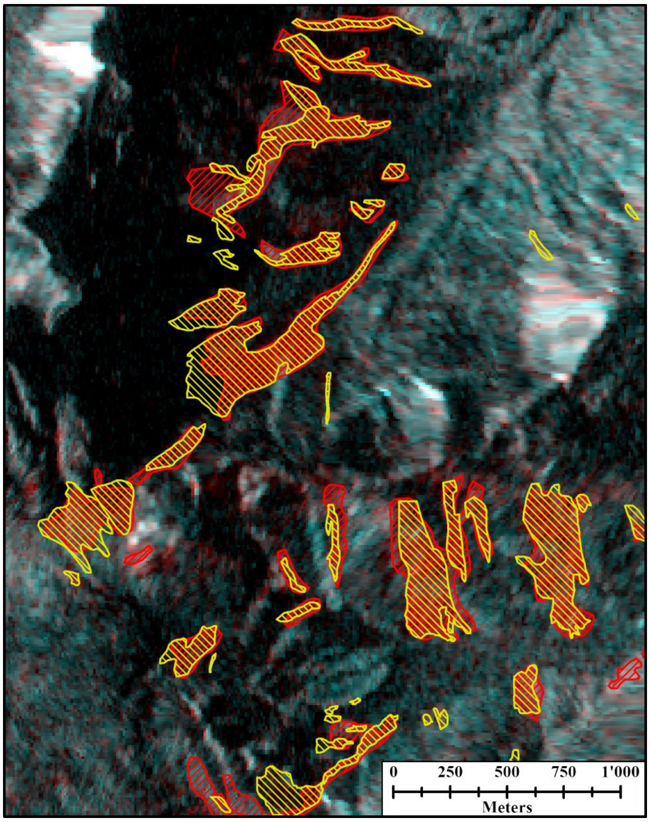

Figure 6. Manually mapped *new* avalanches (in red) from the change detection image S1(12-31 / 01-12) ~~(background)~~ compared to manually mapped *new* avalanches from tsx(12-31 / 01-11) (yellow). No mask is shown for avalanches classified as *old* or *unsure*. ~~Orthorectified with~~ The images from which the masks were derived are shown in Figs. 4a and 4b. Image orthorectified with swissALTI3D © 2019 swisstopo (JD100042), reproduced with the authorisation of swisstopo (JA100120).

~~smaller avalanches are more likely not to be mapped (~~small avalanches (yellow in Fig. 6) are more likely to be missed.

As detailed in Table 4, from the 89 *new* avalanches, 83 were also found by TSX. They correspond to 76 *new* and 7 *unsure* avalanches; 6 avalanches were not found. Vice versa, two thirds (104/164) of the avalanches found in tsx(12-31 / 01-11) correspond to the 83 avalanches also found with S1. One third (60/164) was not found, mostly because they were too small to be detected with S1. We found that the smallest avalanches detected by S1 have an area of around 2000 m^2 (Sect. 5.1).

5.4 Multiorbital S1 change detection composite

By combining S1 acquisitions from multiple ascending and descending orbits, we minimized areas affected by radar ~~shadow and layover~~ layover (areas with radar shadow appear in layover when imaged with the opposite pass direction). The multiorbital change detection composite

Table 4. (a) Number of manually detected *new* avalanches in S1(12-31 / 01-12) which were also detected as *new* or *unsure* in the change detection image tsx(12-31 / 01-11). (b) reverse correspondence.

(a)	of *new* in S1(12-31 / 01-12)	→		tsx(12-31 / 01-11)
	total	found	(*new* / *unsure*)	not found
	89	83	(76 / 7)	6
(b)	of *new* in tsx(12-31 / 01-11)	→		S1(12-31 / 01-12)
	total	found	(*new* / *unsure*)	not found
	164	104	(100 / 4)	60

is shown in Fig. 7 and covers entire Switzerland during the first avalanche period. In the full, non-local mean filtered 15 m-resolution image, which is available online (Leinss et al., 2019), we manually counted 7361 avalanches but did not draw any polygons. We found that avalanches reaching below the wet snow line were much better visible than avalanches from the dry snow zone. ~~Figure 4c shows a subset which~~ The subset shown in Fig. 4c illustrates the mitigation of ~~shadow and layover~~ layover (in the upper and lower right), the speckle reduction and the enhanced resolution compared to the single orbit S1 image in Fig. 4b. Only areas near radar shadow loose contrast and show a reduced avalanche visibility because the added layover image does not contain useful information.

The comparison of the multiorbital S1 mapping results with the high resolution TSX data is detailed in Table 5. In the study area a total of 136 *new* avalanches were manually detected in the multiorbital image (S1-MO). Of these, 104 avalanches match with avalanches detected in the corresponding single orbit TSX change detection scene (95 of them with *new* avalanches, 9 with *unsure*), whereas 32 avalanches were not found with TSX. 17 of the 32 avalanches could not be detected because they are in the shadow/layover areas of TSX. Vice versa, 110 of 164 TSX avalanches were also detected in the multiorbital S1 composite whereas 54 TSX avalanches were not detected.

Table 5. (a) Number of the *new* avalanches in the S1 multiorbital change detection image (S1-MO) compared to avalanches in the TSX change detection image. Reverse correspondence in (b).

(a)	*new* in S1-MO(12-28+4d / 01-09+4d) → tsx(12-31 / 01-11)		
	total	found (*new/unsure*)	not found (in/not in shadow)
	136	104 (95 / 9)	32 (17 / 15)
(b)	*new* in tsx(12-31 / 01-11) → S1-MO(12-28+4d / 01-09+4d)		
	total	found	not found
	164	110	54

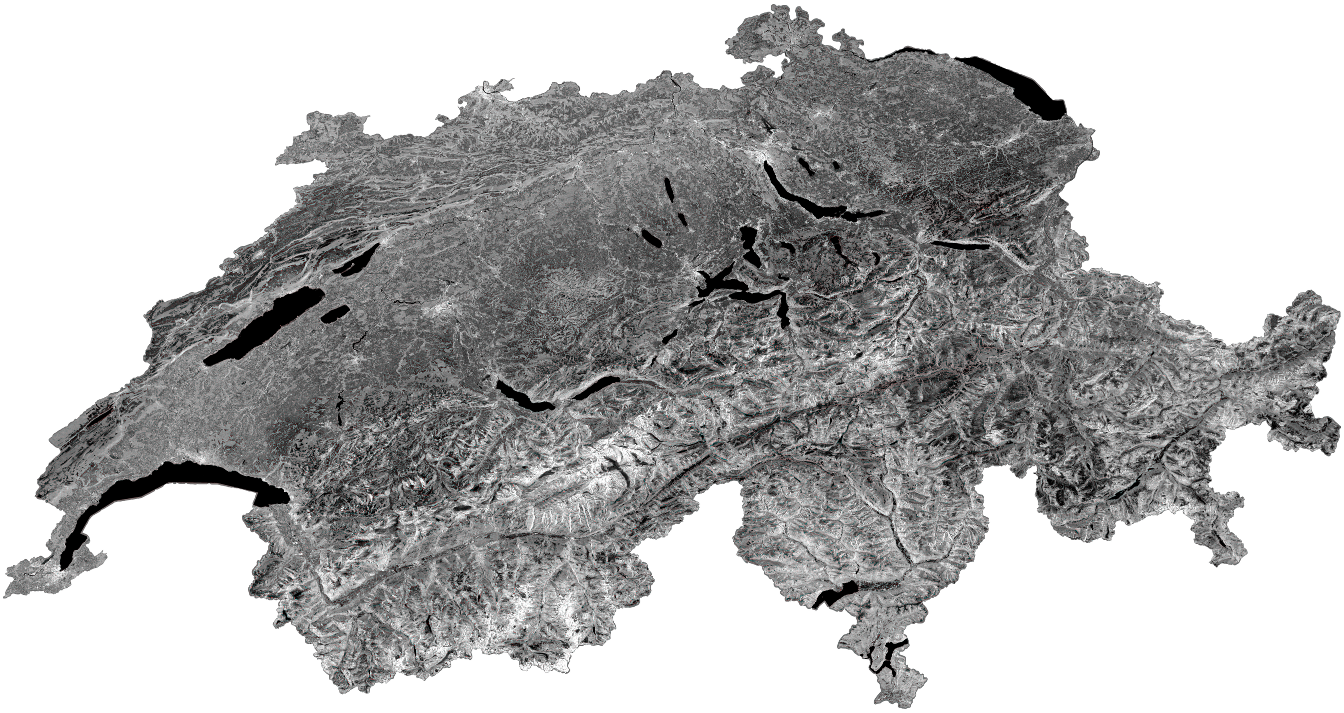

Figure 7. In the 15 m-resolution multiorbital S1 change detection mosaic, covering entire Switzerland for the first avalanche period around Jan 4th, we manually counted 7361 *new* avalanches. When zooming into the image, many avalanches are visible in red. The image is combined from each 12 acquisitions from 2017-12-28 until 2018-01-01 and from 2018-01-09 until 2018-01-12 and is available online (Leinss et al., 2019). All Copernicus Sentinel scenes (2019) were orthorectified with the swissALTI3D © 2019 swisstopo (JD100042), reproduced with the authorisation of swisstopo (JA100120).

5.5 Automated avalanche detection

For the implemented automatic avalanche detection algorithm we chose a threshold of 4 dB for the relative brightness of avalanches which corresponds to the upper 82% of the avalanche brightness distribution shown in Fig. 8a. The figure is based on 99 of 164 *new* avalanches which cover more than 100 pixels (Sect. 4.4) and which were selected from tsx(12-31 / 01-11) . for the entire study area (red rectangle, Fig. 1). The threshold to mask out areas steeper than 35° (Sect. 4.5) is supported by the slope-dependent distribution of avalanche pixels in Fig. 8b. With these settings, the automatic methods identified about two thirds of the manually identified avalanches in the same image pair. Here we considered the manually determined avalanche mask as a proxy for the true extend of the deposition zone. We are aware that the significance of such a comparison is limited. Nevertheless, the advantage of this comparison is that the performance of the detection algorithm is directly compared to the results of a human avalanche mapping expert.

For the first image pair tsx(12-31 / 01-11) Table 6a details that 110 of 164 manually mapped *new* avalanches were also found with the automated detection whereas 54 were not found. As shown in Fig. 9, these "missed" avalanches are often very small avalanches which were filtered out by the algorithm. Vice versa, of 138 automatically detected avalanches 21 were not found manually (Table 6b).

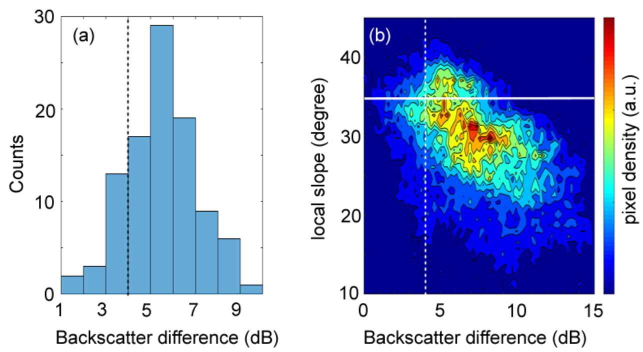

Figure 8. (a) Histogram of the mean relative brightness of avalanches compared to surrounding area for manually mapped *new* avalanches in of tsx(12-31 / 01-11) in the study area (red polygon, Fig. 1). (b): Relative brightness of the avalanche pixels in relation to the local slope angle. Lines indicate the thresholds for the backscatter difference (dashed) and the slope-dependent mask (solid).

When considering the total number (164) of manually detected avalanches (164in the study area (red polygons in Fig. 1) as truth one can assign avalanches which were also found automatically to *true positive* (TP = 110), i.e. correctly

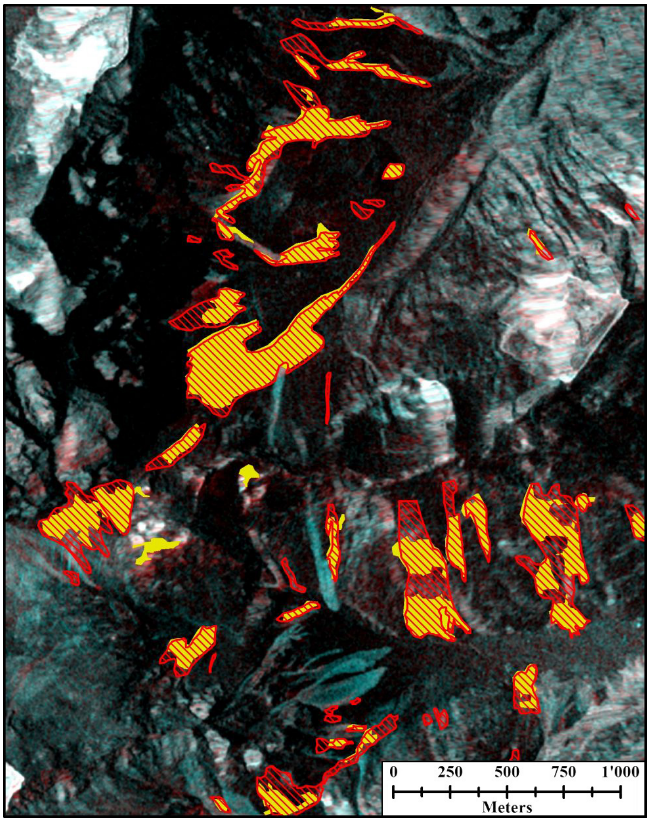

Figure 9. Comparison between detected *new* avalanches when manually mapped (red) and automatically detected (yellow) in the TSX acquisition pair 2017-12-31 vs. 2018-01-11. The TSX background image is shown without mask in Fig. 4a. Orthorectified with the swissALTI3D © 2019 swisstopo (JD100042), reproduced with the authorisation of swisstopo (JA100120).

detected. The remaining avalanches, which were not automatically detected, are then assigned to *false negative* (FN = 54), i.e. incorrectly rejected. With this assumption the probability of detection (POD) and the miss rate or false negative rate (FNR) can be calculated:

$$\mathrm{POD} = \frac{\mathrm{TP}}{\mathrm{TP} + \mathrm{FN}} \quad \text{and} \quad \mathrm{FNR} = \frac{\mathrm{FN}}{\mathrm{TP} + \mathrm{FN}} = 1 - \mathrm{POD} \qquad (3)$$

Further, one can assign automatically detected avalanches which were not manually found to *false positives* (FP = 21), i.e. incorrectly detected. When assuming that the number of correctly detected avalanches is given by TP = 110, the false discovery rate (FDR) reads

$$\mathrm{FDR} = \frac{\mathrm{FP}}{\mathrm{FP} + \mathrm{TP}} \qquad (4)$$

With that one obtains a POD = 67 %, a miss rate FNR = 33 % and a false discovery rate FDR = 16 % for tsx(12-31 / 01-11).

For the second image pair tsx(01-11 / 02-02) only 82 of 170 manually detected *new* avalanches were automatically found whereas 88 were not found (Table 6c). Vice versa, 54/179 automatically detected avalanches were not found manually (Table 6d). Assuming again that the manually detected avalanches are the true avalanches one obtains a POD of 48 %, a FNR of 52 %, and a FDR = 40 %. The results are expected to be worse compared to the first period, because mapping of *new* avalanches was very difficult for the second period where many old and new avalanches overlapped such that many *unsure* cases occurred for which the backscatter signal changed less than the threshold of 4 dB.

The automated algorithm was also run on the S1 images pair S1(12-31 / 01-12). As detailed in Table 6e, 68 of 89 manually detected *new* avalanches were also found automatically whereas 21 were not found. Vice versa, of 92 automatically mapped avalanches 72 were also found manually and 20 were not found (Table 6f), resulting in a POD = 76%, a FNR = 24%, and a FDR = 23%.

The higher POD and lower FNR for S1 compared to TSX indicates only, that with S1 the automatic method can detect a larger fraction of the manually detected avalanches. It does not indicate that results obtained from S1 are better compared to TSX data where in total more avalanches were detected.

Table 6. Number of automatically detected *new* avalanches compared to the number of manually detected *new* avalanches~~from the same image pair~~.

(a)	man:tsx(12-31 / 01-11)		→	auto:tsx(12-31 / 01-11)	
	total	found	POD	not found	FNR
	164	110	67%	54	33%
(b)	auto:tsx(12-31 / 01-11)		→	man:tsx(12-31 / 01-11)	
	total	found		not found	FDR
	138	117		21	16%
(c)	man:tsx(01-11 / 02-02)		→	auto:tsx(01-11 / 02-02)	
	total	found	POD	not found	FNR
	170	82	48%	88	52%
(d)	auto:tsx(01-11 / 02-02)		→	man:tsx(01-11 / 02-02)	
	total	found		not found	FDR
	179	125		54	40%
(e)	man:S1(12-31 / 01-12)		→	auto:S1(12-31 / 01-12)	
	total	found	POD	not found	FNR
	89	68	76%	21	24%
(f)	auto:S1(12-31 / 01-12)		→	man:S1(12-31 / 01-12)	
	total	found		not found	FDR
	92	72		20	23%

6 ~~Discussion~~

5.1 Size distribution of detected avalanches

5.2 ~~Advantage of radar change detection images~~

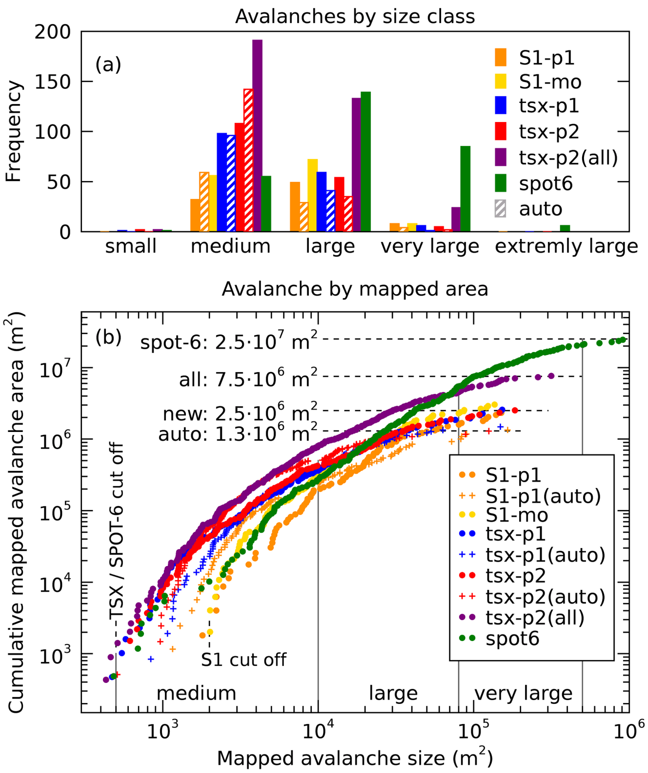

Figure 10. (a): Classification of mapped avalanche area into size classes. (b): the cumulative avalanche area $\Sigma_1^i A_i$ plotted over avalanche size (A_i) reveals that the smallest avalanches size detected by TSX and SPOT-6 is about $500\,\mathrm{m}^2$, $2000\,\mathrm{m}^2$ for S1, and around $1000\,\mathrm{m}^2$ for the automatic methods. The total cumulative areas differ by an order of magnitude: with radar only bright deposit areas of *new* avalanches were mapped automatically ($1.3 \cdot 10^6$ m^2), and less-bright areas were added manually ($2.5 \cdot 10^6$ m^2). Summing all classes (*new, old, unsure*) in TSX images results in $7.5 \cdot 10^6$ m^2 which is one third of the cumulative area of SPOT-6 outlines ($2.5 \cdot 10^7$ m^2) which cover also older avalanches and for which outlines of the entire avalanche area (release, path, deposit) were either clearly visible or were at least estimated.

~~In both high resolution TSX stripmap radar images more than one hundred avalanches have been manually detected by visual inspection of single radar images within the analyzed area covering .However, a clear advantage has been found when using successive images for change detection where about twice as much avalanches could be differentiated (Sect. ??~~The size distribution of detected avalanches depends on sensor resolution and also on which features are actually visible by the sensor. For radar sensors it is likely that only the deposit area is mapped, whereas for the SPOT-6 dataset care was taken to map (or at least estimate) the entire avalanche area, including the release area (Sect. 5.2). Because with radar only partial areas were mapped, simple size distributions (Fig. 10a) may appear shifted. To provide more detailed insight we plotted the cumulative area $\Sigma_1^i A_i$ of all avalanches sorted by their apparent area A_i (Fig. 10b).

~~Additionally, change detection images provide a temporal information which~~ The smallest detectable avalanche size can be found in the lower tail of the curves in Fig. 10b: for TSX and SPOT-6 the smallest avalanches have about $500\,\mathrm{m}^2$, $2000\,\mathrm{m}^2$ for S1, and around $1000\,\mathrm{m}^2$ for the automatic methods.

It may surprise that in the study region the total avalanche area in SPOT-6 images is an order of magnitude larger ($2.5 \cdot 10^7$ m^2 , green curve in Fig. 10b) than the total area of manually radar-detected *new* avalanches from TSX and S1 (red, blue, and orange dots: $2.5 \cdot 10^6$ m^2). A factor of three remains when comparing the area of all (*new, old*, and *unsure*) avalanches detected by TSX (purple in Fig. 10b) with SPOT-6 which does not contain any age classification. Considering the fact that with radar mainly the deposition zone can be mapped a difference of a factor of three is reasonable.

6 Discussion

6.1 Radar change detection images

The temporal information from radar change detection makes it possible to differentiate relatively clearly between new and old avalanches. ~~Therefore, they can be much easier differentiated from bright regions of similar shape but which are in reality erosion features like scree or talus deposits and which do not significantly change their backscatter behavior in time (therefore classified as *unsure*) . Still, ~~, at least for low avalanche activity where old avalanches are rarely overrun by new ones. This can be seen as a major advantage compared to optical images for which temporally dense time series are not reliably available due to weather conditions. The missing temporal information can lead to an overestimation of the avalanche area and (Bühler et al., 2019) report that deposit areas of large avalanches ($> 10\,000$ m^2) remain visible for several weeks.

Nevertheless, for strong avalanche activity, the differentiation of ~~strongly~~ overlapping avalanches is difficult ~~and requires a high spatial and temporal resolution. In the extreme case, a temporal resolution of seconds or minutes would be required to temporally resolve individual avalanches . The~~ even with radar. For example, we found a large number of *unsure* avalanches for the second analyzed avalanche event (Sect. 5.1) which could be assigned to *new* avalanches of the first event. For temporal separation, fast repeat times of current radar satellites, like 6 days when combining the two S1 satellites is a major advantage compared to other ~~mapping methods. For example, compared to the 11 days of TSX, the temporal resolution of S1 is almost twice as high. Due to clouds, optical data is not reliably available and temporally dense time series cannot exist for weather conditions with heavy snow fall and strong winds during which the highest avalanche risk occurs.~~ satellites (TSX: 11 days, Radarsat: 24 days). To differentiate overlapping avalanches a recently developed age-tracking algorithm showed promising results (Eckerstorfer et al., 2019).

6.2 Optical mapping vs. radar change detection

Regardless of the advantages of radar change detection, the spatial resolution of optical sensors is better compared to ~~radar sensors of the same nominal resolution~~ the nominal resolution of radar sensors because the intrinsically coherent SAR imaging method makes radar speckle unavoidable and requires spatial or temporal averaging. Furthermore, the resolution of TSX and S1 is not good enough to recognize flow structures of the avalanche surface which are well visible in the optical SPOT-6 images (Bühler et al., 2019).

~~With~~ Nevertheless, using TSX change detection ~~images~~ we have mapped a similar number of avalanches (316) compared to the results from optical SPOT-6 images (286 avalanches) within the ~~analyzed~~ study area. However, the mapped avalanche outlines differ relatively strongly and are sometimes split up into sub-polygons which results in the fact that only 68% of the radar detected avalanches overlap with avalanches found with the optical data or inversely, only 44% of optically detected avalanches were also found by radar. The differences of ~~the~~ avalanche outlines could also be partially attributed to the ~~estimation of avalanche outlines by the person~~ fact that some avalanche outlines were estimated by the (different) persons mapping the avalanches.

The fact that a larger fraction (68% vs. 44%) of radar-detected avalanches matches with optically detected ones results from the better differentiation of adjacent avalanches into multiple classes (*new, old, unsure*) which ~~have been~~ were often mapped as one large avalanche with optical data. When multitemporal optical data is available, a temporal differentiation is also possible (Bühler et al., 2019) which, however, was done for a different region than our analyzed area.

From the analysis of avalanches detected by radar but not found in the optical SPOT-6 image, we found that more than 80% of these avalanches were located in the cast shadow. ~~It seems that these avalanches are not easy to detect in the optical images whereas they are well visible in radar images.~~ Similar, in radar images no information is available from the radar shadow and very poor information is available from layover areas, however, only 35% of avalanches not found in the radar images (but in optical) are located in the radar shadow or layover. We think it is an important result that not only radar acquisitions are affected by (radar) shadow but that avalanche mapping ~~results with~~ using optical data seem also to be deteriorated by the cast shadow from high mountains.

~~Unfortunately,~~ A main difference between SPOT-6 and radar mapping results is that the total avalanche area differed at least by a factor of three (Fig. 10b). We attribute this difference to the fact with SPOT-6 avalanches were mapped more completely (origin, path, deposition zone) than with radar (mainly deposition zone). This has important consequences when comparing avalanches by pixel area rather than by overlap.

Due to unfortunate acquisition timing, the direct comparison of SPOT-6 and TSX data is ~~limited by several uncertainties: the acquisition date of the~~ not ideal: the SPOT-6 images (2018-01-24) was acquired just between the two TSX images (2018-01-11~~and~~ , 2018-02-02) ~~and~~ which leaves 9 days where additional avalanches could have occurred, considering about 20 cm of fresh snow on Feb 1st. Nevertheless, Fig. 2 indicates that the biggest part of avalanches occurred before the SPOT-6 acquisition and only about 5% of avalanches occurred ~~between the SPOT-6 and the TSX acquisition from~~ until Feb 2nd. ~~To confirm this we analyzed~~ We confirm this by analyzing a multiorbital S1 change detection image S1(01-24+01-28 / 01-30+02-03) ~~and~~ where we did not find any new avalanches in the study area. ~~As the avalanche risk was slightly higher (level 2–3) for north exposed slopes after Jan (SLF, 2018c, d) we cannot completely exclude that during this time an unknown amount of avalanches too small to be detected by S1 could have still released in the case shadow.~~

6.3 TSX compared to S1 change detection

The comparison of TSX and S1 change detection images, both of them acquired for the first avalanche period with almost identical orbits and acquisition times, shows that the S1 satellites are a valuable source of radar images for avalanche mapping. ~~Though with~~ The size of smallest detectable avalanches for TSX are "medium" avalanches (500 – 10 000 m^2) with a width of more than 20 m. S1 ~~very small avalanches are likely to be missed.~~ misses mainly "medium" avalanches smaller than 2 000 m^2 (Fig. 10b). Similar results for S1 with a minimum cutoff of 4 000 m^2 were found by Eckerstorfer et al. (2019).

Still about two thirds of avalanches detected and classified as *new* with TSX could also be detected with S1 (Sect. 5.3).

Notably, 93% (83/89) of avalanches detected by S1 could also be detected by TSX which reflects the agreement between TSX and S1 mapping results. This is confirmed by Fig. 10b which shows that, despite of a different lower cut off, the total area of radar-mapped *new* avalanches agrees very well ($2.5 \cdot 10^6$ m^2). Also, the shape of the avalanches masked in S1 data is very similar to the one from TSX (Fig. 6). Therefore, we consider the reduced resolution and separability of avalanches in S1 images to be much less relevant than the superior availability of S1 data.

6.4 Multiorbital composite

The combination of radar ~~acquisitions~~ images acquired with different polarizations and from ascending and descending orbits ~~minimizes~~ reduced radar speckle and minimized areas affected by ~~radar shadow and layoverand reduces speckle noise. Noise was further reduces by averaging both polarizations (VV, VH) available from the dual-polarization S1 data. By combining the two orbit directions and the two~~ layover. By combining two orbit and (pairwise incoherent) polarizations, areas visible from both orbits were imaged by 4 independent observations. ~~This number can~~ In our case of mapping entire Switzerland for a specific period, this number was even increase to 6 or 8 observations when acquisitions with different incidence angles (from the same orbit direction) overlap. Due to the 4–8 independent observations, spatial multilooking (used for speckle reduction) could be reduced to 4×1 pixels to obtain a radiometric accuracy otherwise only possible with multilooking windows of $8...16 \times 2$ pixels. With this multiorbital averaging method, we estimate that an effective spatial resolution of about 20×20 m was achieved (TSX: about 10×10 m after multilooking). This resolution enhancement can be clearly observed when comparing Fig. 4b with Fig. 4c. ~~Still, these values hold only for flat terrain.For geometric reasons the local resolution $\delta_{\mathrm{rg}} = \delta_{\mathrm{sr}}/\cos\theta$ of mountain slopes depends on the local incidence angle θ such that, compared to flat terrain, slopes~~ Also, about twice as much medium size avalanches were detected compared to a single S1 image (Fig. 10a). However, because topography was not considered during averaging the resolution can deteriorate in slopes facing off the radar ~~show an increased resolution whereas slopes facing away from the radar show a significantly deteriorated image quality or even complete loss of resolution in the case of layover~~(Sect. 3).

Another drawback of combining acquisitions from multiple dates is that no unique time stamp can be given to the "before"- and "after"-aquisition. In the worst case, avalanches loose contrast if they had occurred during the collection period of the set of "before" images. However, in our case, we focused on the extreme avalanche event on 2018-01-04 (Fig. 2) and made sure that the "before"- and "after"-imaging period did not overlap with the main avalanche event. For an operational use combined (asc+desc) acquisitions must be acquired within a time-period as short as possible, i.e. significantly shorter than the orbit revisit time to avoid reduced visibility by averaging out "in-between" avalanches which are only visible in one of the two averaged acquisitions. For S1, ascending and descending acquisitions with only 12 hours time difference should be used, if possible. Considering a revisit time of 6 days over Europe results in probability of 1:12 to reduce the visibility of averaged avalanches.

~~To combine multiple orbits~~ In this study we simply averaged the change detection radar images ~~in dB which preserved the relative brightness and resolution of local features (avalanches). By the simple average slopes facing off the radar were mainly lightened up by the average with a bright layover area.~~ and did not apply any terrain correction. We think that more advanced methods to merge radar images from multiple orbits, for example local resolution weighting (LRW) by Small (2012), should further improve avalanche mapping results.

From the comparison to optical data we also found that avalanches can be clearer identified in slopes facing off the radar compared to slopes which are facing towards the radar (but not yet in layover). As detailed in Sect. 3, we think that, because of the more isotropic scattering ~~of the rough surface of avalanches steep~~ from the rough avalanche debris surface, steep local radar incidence angles should be used to enhance the local contrast to the surrounding snow. Therefore, slopes facing away from the sensor should be given more weight which is ~~implicitly already done~~ done already implicitly by LRW. Furthermore, in mountainous regions LRW applies already unequal weights for ascending and descending acquisitions which decreases further the probability that avalanche falling inbetween the averaged acquisitions loose their visibility.

~~The additionally applied non-local mean filter further increased the visibility of avalanches (compare Fig. 4c with Fig. 4d). The enhanced geometric and radiometric resolution through multiple orbits and the non-local-mean filter makes the separability of avalanches in S1 data almost equivalent to single-orbit and single-polarization TSX data (Sect. 5.4). This conclusion is also supported by the avalanche differentiation ratio of 1.06 (Table 7) which is discussed in Sect. 6.6.~~

6.5 Automated avalanche detection

For both, TSX and S1 images the implemented avalanche detection algorithm performs with reasonable results, at least when the number of overlapping avalanches is low. ~~As shown in~~ That means that in general a few sparse events are more likely to be detected than overlapping clusters of avalanches.

Compared to the manually detected avalanches (red shading in Fig. 9), the area of automatically detected avalanches (yellow) shows a good agreement~~with manually~~

Table 7. Avalanche differentiation ratios between different satellite acquisitions and methods, and mutual miss-/false discovery rates.

~~tsx(12-31 / 01-11) TSX(01-11) 1.10 33% 8%tsx(01-11 / 02-02) TSX(02-02) 1.39 31% 5%~~

Set A	Set B	$\frac{N_{A\to B}}{N_{B\to A}}$	$\frac{N_{A\neg B}}{N_A}$	$\frac{N_{B\neg A}}{N_B}$
tsx(12-31 / 01-11)	SPOT-6 (01-24)	1.72	32%	56
tsx(12-31 / 01-11)	S1(12-31/01-12)	1.25	37%	7
tsx(12-31 / 01-11)	S1-MO	1.06	33%	24
tsx(12-31 / 01-11)	manual vs. auto	0.94	33%	15
S1(12-31 / 01-12)	manual vs. auto	0.94	24%	22
tsx(01-11 / 02-02)	manual vs. auto	0.66	52%	30

~~detected avalanches (red shading)~~. However, the upslope parts of avalanches are often only fractionally detected because of their relatively low brightness. For a weakly visible starting or transition zone a human observer can conclude that it must belong to the below situated avalanche deposit. Also, by choosing a threshold of 4 dB already 18 % of the manually detected avalanches are likely to be missed (Fig. 8a). A dynamic threshold based on backscatter changes in individual image pairs could improve these results (Eckerstorfer et al., 2019). Further, minor parts of manually detected avalanches are located in slopes steeper than 35° (Fig. 8b) which were masked out by the automatic method.

6.6 Avalanche differentiation with different methods

The fact that no real ground truth exists makes a direct comparison of the different methods difficult. However, some methods show a much higher potential to differentiate ~~avalanches than others. Because of the better differentiation, the quantitative comparison of found avalanches should be interpreted with the consideration that multiple avalanches can correspond to a single, big avalanche~~large connected avalanche patches into multiple smaller ones than other methods. Therefore we use a reciprocal, two-way comparison of avalanche detection numbers to estimate which of the methods can better differentiate adjacent avalanches.

As a proxy for the enhanced differentiation we define the ratio $N_{A\to B}/N_{B\to A}$ where $N_{A\to B}$ is the number of avalanches from data set A which were also found in the data set B, and inversely, $N_{B\to A}$ is the number of avalanches in B which were also found in A. Additionally, we define the ratio $N_{A\neg B}/N_A$ of avalanches found in A but not found in B relative to all avalanches found in A and analogue $N_{B\neg A}/N_B$. The meaning of the last two ratios depends on interpretation and correspond to the false discovery rate (FDR) under the assumption that B is considered as truth or alternatively to the false negative rate (FNR) if A is considered as truth.

Table 7 lists the three ratios for different data sets. We interpret these numbers such that a differentiation ratio $\frac{N_{A\to B}}{N_{B\to A}} > 1$ indicates that set A provides spatially more detailed results than set B. An asymmetry between the last two columns indicates that one method detects more avalanches than the other method.

~~From the first two rows of Table 7, derived from *new* avalanches in Table ??, we conclude that with change detection avalanches are better to differentiate and that more than 30% of *new* avalanches can be detected compared to mapping using single images. We also conclude that the miss-detection rate of single images is relatively low (5-8%).~~

From the comparison to ~~SPOT-6~~SPOT-6, derived from Table 3, we infer that TSX change detection allows for a better differentiation of avalanches than single optical images. However, both methods show miss rates (and possibly some false detection) of 32 and 56% for avalanches which are not visible by the other method which indicates a certain complementarity of optical and radar images for avalanche detection.

Compared to S1, the higher resolution of TSX allows for a 25% better differentiation and 37% more avalanches were detected (derived from Table 4). Still, the false discovery rate of S1 compared to TSX is quite low (7%).

Interestingly, the avalanche separability of the multiorbital S1 composite, including the NL mean filter, is very comparable to TSX single orbit change detection (1.06) while 33% or 24% of avalanches detected by one method are not visible with the other (derived from Table 5). This, because TSX detects smaller avalanches, while the multiorbital methods detects also avalanches which are otherwise in ~~the radar shadow or in slopes facing the radar~~slopes close to layover.

Finally, the automatic methods ~~detects~~ detect larger avalanches fairly comparably to the manual method (derived from Table 6), however, weakly visible avalanches and small avalanches which have not been automatically detected cause a miss rate of about 30 %. The apparently lower differentiation of avalanche by manual analysis results from the fact that the automatic method often detects multiple patches instead of a single avalanche (Fig. 9).

7 Conclusions

We studied the capabilities of the radar satellites TerraSAR-X (TSX) and Sentinel-1 (S1) to detect avalanches ~~using single radar images,~~ in two-image change detection images and multiorbital change detection composites. Manual avalanche mapping results from the high- and medium resolution radar data (TSX, S1) and high resolution optical data (~~SPOT-6~~SPOT-6) were compared to each other. An automatic detection method was developed and compared to the manual mapping results.

We conclude that both, TSX and S1 radar images can provide valuable, weather-independent information about avalanche activity, even in difficult alpine terrain. ~~We showed that avalanches can be manually identified in single radar images, but the mapping precision is significantly enhanced~~

~~and a temporal information is added when two consecutive radar images are combined into an RGB change detection image. With that~~ Despite of different lower cut-off sizes of about 500 m^2 for TSX and 2000 m^2 for S1, avalanche outlines and the total area of mapped avalanches agree very well with each other.

Between the manual TSX and SPOT-6 mapping results, we found a fair agreement ~~between TSX results and mapping from single~~ but the total mapped avalanche area of TSX covers only one third (the deposition zone) of the total mapped area (release, path, deposit) in SPOT-6 images. Interestingly, many avalanches located in the cast shadow of SPOT-6 image were not detected ~~in the optical SPOT-6 image~~ whereas they were clearly visible in a TSX image acquired 10 days later. With the automated detection algorithm we found about 60–80% of the avalanches manually mapped in the same image, at least when no large number of old avalanches were present.

~~Despite of the high resolution of TSX which allows for a more detailed avalanche mapping, the~~ We found that the non-systematic acquisition program and the possibly high cost can be considered as drawback of TSX data. Also, with the maximal swath width of 30 km in stripmap mode and a nominal revisiting period of 11 days, an operational use for avalanche mapping over Switzerland with TSX is not feasible. However, ~~high resolution radar from TSX~~ the high resolution images can provide valuable information for validation of lower resolution mapping results for pre-defined test sites and if acquisitions are scheduled in advance.

~~In contrast to TSX, and despite of its~~ Despite of the lower resolution, we found that S1 provides a convincing solution for systematic avalanche mapping because of the total swath width of 250 km and the revisit period of 6 days when images from the same orbit of both satellites (S1-A and S1-B) are combined. The results from Norway by ~~Eckerstorfer et al. (2018)~~ Eckerstorfer et al. (2018, 2019) confirm this conclusion. ~~For a selected test site we detected with S1 about two thirds of the avalanches found with TSX but small avalanches were often missed. With the~~

With the multiorbital combination of systematically available S1 acquisitions from different orbits and with different polarizations we minimized not only areas located in radar ~~shadow and~~ layover but also enhanced the radiometric accuracy and obtained a high spatial resolution of about 20 × 20 m. In the resulting change detection image covering entire Switzerland we ~~found~~ manually counted in total 7361 new avalanches which occurred during an extreme avalanche period around January 4th 2018. However, we suppose that mainly avalanches reaching below the wet snow line were detected and that likely many dry snow avalanches were missed because of their lower contrast to the surrounding snow. A disadvantage of the multiorbital composite is the loss of precise timing of avalanches. For operational applications we suggest therefore to minimize the ratio of elapsed time between ascending and descending acquisitions and of the revisit time.

We think that avalanche mapping can be ~~even~~ further improved with more advanced methods to combine different orbits, for example with local resolution weighing, LRW (Small, 2012). With that, slopes facing off the radar are weighted stronger which does not only enhance the resolution but should also increase the avalanche visibility~~as~~ : we think that the more omnidirectional scattering of the rough avalanche surface dominates the scattering of smooth snow only for slopes facing off the radar. We found that avalanches are hardly visible in slopes facing the radar (but not yet in layover). As with LRW mountain slopes are unequally weighted the probability that avalanches occur between two averaged images is reduced.

Although we could show that radar change detection mapping with TSX provides results comparable to optical SPOT-6 direct mapping, we note that our study focuses on the exceptionally warm January 2018 with frequent surface melt but also with very intense snowfall periods. As the relative brightness of avalanches with respect to the surrounding snow depends on the water content and the amount of deposited snow, avalanches might be less visible during cold weather with little snowfall. Therefore, we think that ~~the~~ an analysis of longer time series of radar based avalanche mapping ~~is required to assess~~ will provide insight how snow and weather conditions affect the detection rate of radar based methods~~under different weather conditions and in different regions~~.

Data availability. TerraSAR-X data are available from the archive https://terrasar-x-archive.terrasar.com. Copernicus Sentinel-1 data processed by ESA have been downloaded from the Copernicus Open Access Hub: https://scihub.copernicus.eu and from the Alaska SAR Facility ASF DAAC 2018 https://www.asf.alaska.edu. The manual mapping results from the optical data and the Sentinel-1 change detection composite of Switzerland is available online (Hafner and Bühler, 2019; Leinss et al., 2019).

Appendix A

Author contributions. SL and RW wrote the manuscript, RW did the avalanches mapping and designed the automatic detection. SL coordinated the study and implemented the nonlocal mean filter. SH, SB, SL preprocessed the radar images. YB initiated the study and complemented the manuscript.

Competing interests. The authors declare that they have no conflict of interest.

Table A1. List of S1 acquisitions used for the multiorbital RGB change detection composite shown in Fig. 7.

Satellite	Date	Time (UTC)	rel. orbit, direction
Sentinel-1B	2017-12-28	05:42:17	139, descending
Sentinel-1B	2017-12-28	05:42:43	139, descending
Sentinel-1A	2017-12-29	05:34:45	66, descending
Sentinel-1A	2017-12-29	05:35:10	66, descending
Sentinel-1B	2017-12-30	05:26:02	168, descending
Sentinel-1B	2017-12-30	05:26:27	168, descending
Sentinel-1A	2017-12-30	17:23:14	88, ascending
Sentinel-1A	2017-12-30	17:23:39	88, ascending
Sentinel-1B	2017-12-31	17:14:13	15, ascending
Sentinel-1B	2017-12-31	17:14:38	15, ascending
Sentinel-1A	2018-01-01	17:06:47	117, ascending
Sentinel-1A	2018-01-01	17:07:12	117, ascending
Sentinel-1B	2018-01-09	05:42:17	139, descending
Sentinel-1B	2018-01-09	05:42:42	139, descending
Sentinel-1A	2018-01-10	05:34:45	66, descending
Sentinel-1A	2018-01-10	05:35:10	66, descending
Sentinel-1B	2018-01-11	05:26:01	168, descending
Sentinel-1B	2018-01-11	05:26:26	168, descending
Sentinel-1A	2018-01-11	17:23:14	88, ascending
Sentinel-1A	2018-01-11	17:23:39	88, ascending
Sentinel-1B	2018-01-12	17:14:13	15, ascending
Sentinel-1B	2018-01-12	17:14:38	15, ascending
Sentinel-1A	2018-01-13	17:06:47	117, ascending
Sentinel-1A	2018-01-13	17:07:12	117, ascending

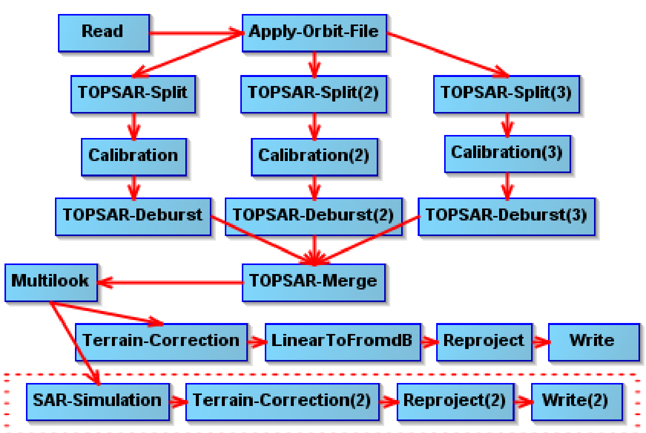

Figure A1. SNAP workflow to process S1 data. The red dashed box is used for creation of the layover and shadow map.

Acknowledgements. We thank Elisabeth Hafner from SLF for providing the manual avalanche mask from the optical SPOT-6 data. Lanqing Huang assisted SH to process the S1 data. We are deeply grateful to Irena Hajnsek from ETH Zürich for providing the working environment, the computational resources and her interest for this work. TerraSAR-X data are provided by the German Aerospace Center (Proposal ID: LAN3585). Meteorological data are provided by the Swiss Federal Office of Meteorology and Climatology (MeteoSwiss).

References

Abermann, J., Eckerstorfer, M., Malnes, E., and Hansen, B. U.: A large wet snow avalanche cycle in West Greenland quantified using remote sensing and in situ observations, Natural Hazards, 97, 517–534, https://doi.org/10.1007/s11069-019-03655-8, 2019.

Bühler, Y., Hüni, A., Meister, R., Christen, M., and Kellenberger, T.: Automated detection and mapping of avalanche deposits using airborne optical remote sensing data, Cold Regions Science and Technology, 57, 99–106, https://doi.org/10.1016/j.coldregions.2009.02.007, 2009.

Bühler, Y., Hafner, E. D., Zweifel, B., Zesiger, M., and Heisig, H.: Where are the avalanches? Rapid SPOT6 satellite data acquisition to map an extreme avalanche period over the Swiss Alps, The Cryosphere, 13, 3225–3238, https://doi.org/10.5194/tc-13-3225-2019, 2019.

Bühler, Y., Bieler, C., Pielmeier, C., Frauenfelder, R., Jaedicke, C., Schwaizer, G., Wiesmann, A., and Caduff, R.: Final Report: Improved Alpine Avalanche Forecast Service AAF, techreport, European Space Agency ESA, 2014.

Condat, L.: A Simple Trick to Speed Up the Non-Local Means, https://hal.archives-ouvertes.fr/hal-00512801, working paper or preprint, 2010.

Cumming, W. A.: The Dielectric Properties of Ice and Snow at 3.2 Centimeters, Journal of Applied Physics, 23, 768–773, https://doi.org/10.1063/1.1702299, 10.1063/1.1702299, 1952.

Davidson, M., Snoeij, P., Attema, E., Rommen, B., Floury, N., Levrini, G., and Duesmann, B.: Sentinel-1 Mission Overview, in: 2009 IEEE International Geoscience and Remote Sensing Symposium, vol. 1, pp. 1–4, https://doi.org/10.1109/IGARSS.2009.5416921, 2010.

Di Tommaso, P., Floden, E. W., Barja, P. P., Palumbo, E., and Notredame, C.: Nextflow enables reproducible computational workflows, Nature Biotechnology, 35, 316–319, https://doi.org/10.1038/nbt.3820, 2017.

Eckerstorfer, M. and Malnes, E.: Manual detection of snow avalanche debris using high-resolution Radarsat-2 SAR images, Cold Regions Science and Technology, 120, 205 – 218, https://doi.org/10.1016/j.coldregions.2015.08.016, http://www.sciencedirect.com/science/article/pii/S0165232X15002037, 2015.

Eckerstorfer, M., Bühler, Y., Frauenfelder, R., and Malnes, E.: Remote sensing of snow avalanches: Recent advances, potential, and limitations, Cold Regions Science and Technology, 121, 126–140, https://doi.org/10.1016/j.coldregions.2015.11.001, 2016.

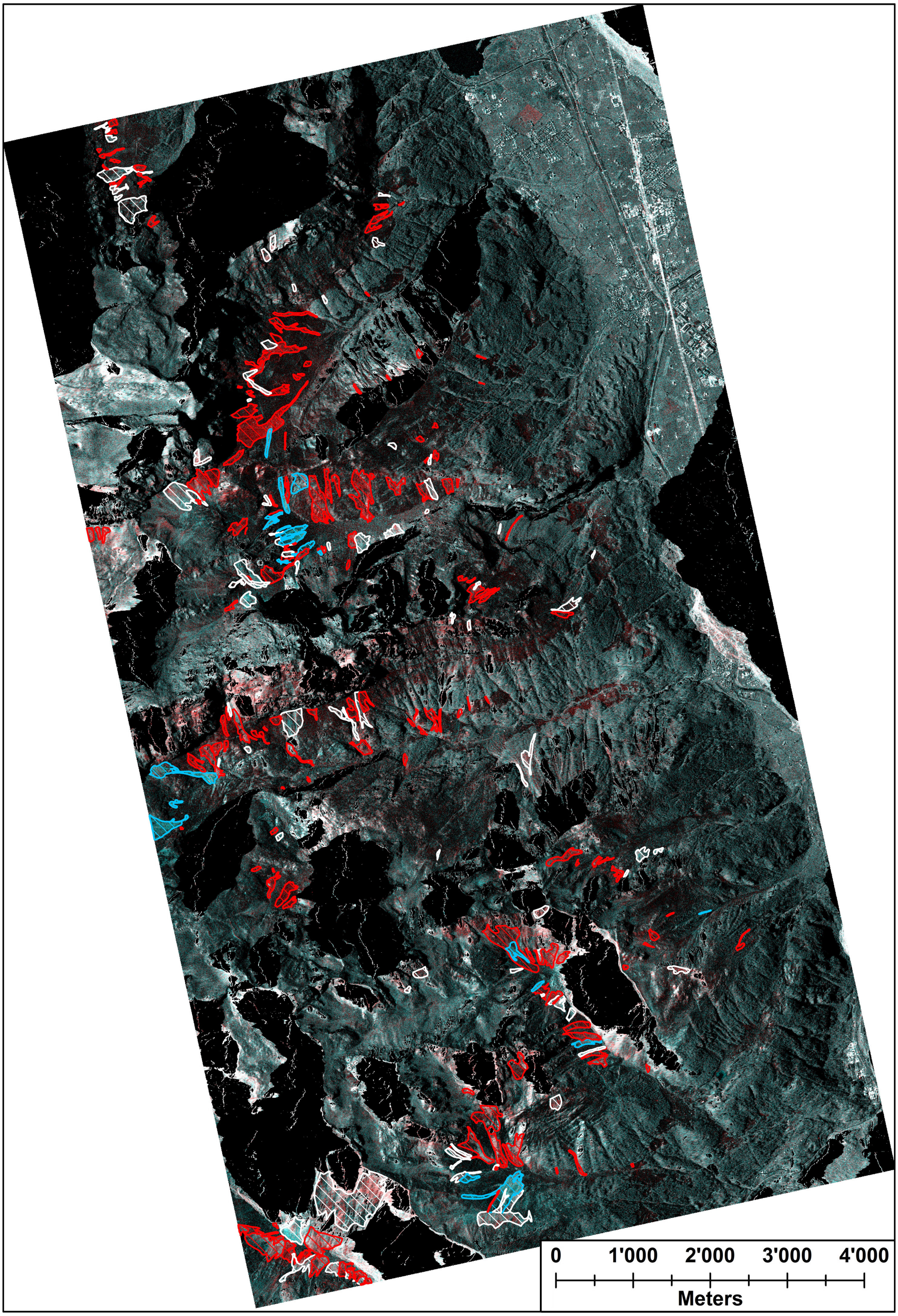

Figure A2. Full extent of the RGB composite image TSX 2017-31-12 vs. 2018-01-11 with manually mapped avalanches. *New* avalanches are red, *old* avalanches blue and *unsure* avalanches white. Areas in the radar layover and shadow are masked out (black). TerraSAR-X image orthorectified with the swissALTI3D © 2019 swisstopo (JD100042), reproduced with the authorisation of swisstopo (JA100120).

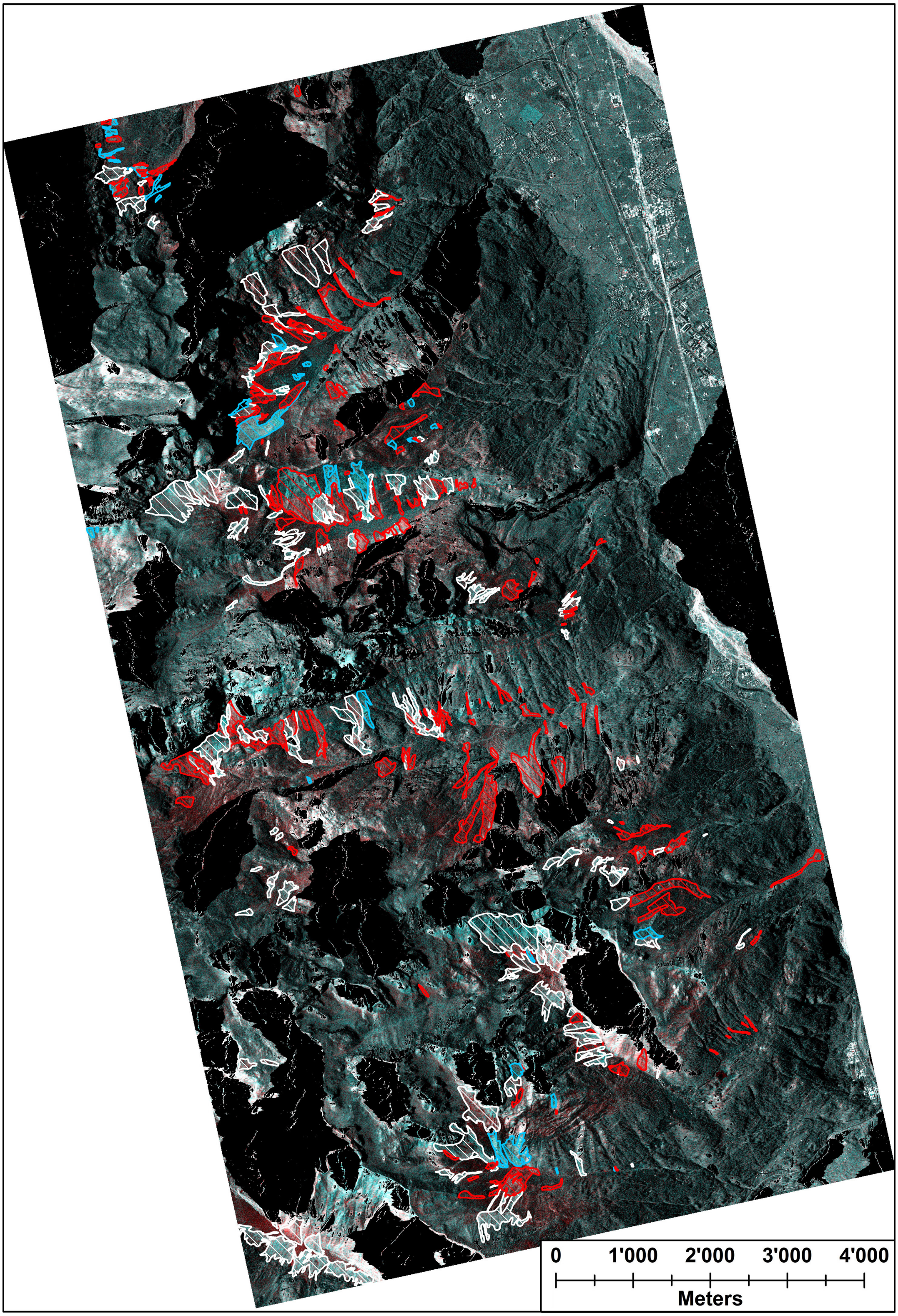

Figure A3. Full extent of the RGB composite image TSX 2018-01-11 vs. 2018-02-02 with manually mapped avalanches. *New* avalanches are red, *old* avalanches blue and *unsure* avalanches white. Areas in the radar layover and shadow are masked out (black). TerraSAR-X image orthorectified with the swissALTI3D © 2019 swisstopo (JD100042), reproduced with the authorisation of swisstopo (JA100120).

Eckerstorfer, M., Malnes, E., and Müller, K.: A complete snow avalanche activity record from a Norwegian forecasting region using Sentinel-1 satellite-radar data, Cold Regions Science and Technology, 144, 39–51, https://doi.org/10.1016/j.coldregions.2017.08.004, international Snow Science Workshop 2016 Breckenridge, 2017.

Eckerstorfer, M., Malnes, E., Vickers, H., Müller, K., Engeset, R., and Humstad, T.: Operational avalanche activity monitoring using radar satellites: From Norway to worldwide assistance in avalanche forecasting, in: International Snow Science Workshop, At Innsbruck, Austria, 2018.

Eckerstorfer, M., Vickers, H., Malnes, E., and Grahn, J.: Near-Real Time Automatic Snow Avalanche Activity Monitoring System Using Sentinel-1 SAR Data in Norway, Remote Sensing, 11, https://doi.org/10.3390/rs11232863, 2019.

ESA: Sentinel-1: ESA's Radar Observatory Mission for GMES Operational Services (ESA SP-1322/1, March 2012), Tech. rep., ESA, 2012.

Frauenfelder, R., Malnes, E., Solberg, R., and Müller, K.: Towards an automated snow property and avalanche mapping system (ASAM), techreport 20130092-04-R, Norwegian Geotechnical Institute NGI, 2015.

Fung, A. K. and Eom, H. J.: Application of a Combined Rough Surface And Volume Scattering Theory to Sea Ice And Snow Backscatter, IEEE Transactions on Geoscience and Remote Sensing, GE-20, 528–536, 1982.

Hafner, E. and Bühler, Y.: SPOT6 Avalanche outlines 24 January 2018, https://doi.org/10.16904/envidat.77, 2019.

Hamar, J. B., Salberg, A., and Ardelean, F.: Automatic detection and mapping of avalanches in SAR images, in: 2016 IEEE International Geoscience and Remote Sensing Symposium (IGARSS), pp. 689–692, https://doi.org/10.1109/IGARSS.2016.7729173, 2016.

International Commission of Snow and Ice: Avalanche atlas: illustrated international avalanche classification, Unesco Paris, https://unesdoc.unesco.org/ark:/48223/pf0000048004, 1981.

Jin, Q., Grama, I., and Liu, Q.: Removing Gaussian Noise by Optimization of Weights in Non-Local Means, 2012 Symposium on Photonics and Optoelectronics, SOPO 2012, https://doi.org/10.1109/SOPO.2012.6270436, 2011.

Karbou, F., Coléou, C., Lefort, M., Deschatres, M., Eckert, N., Martin, R., Charvet, G., and Dufour, A.: Monitoring avalanche debris in the French mountains using SAR observations from Sentinel-1 satellites, in: Proceedings of the International Snow Science Workshop, 1, pp. 344–347, 2018.

Kendra, J. R., Sarabandi, K., and Ulaby, F. T.: Radar measurements of snow: experiment and analysis, IEEE Transactions on Geoscience and Remote Sensing, 36, 864–879, 1998.

Korzeniowska, K., Bühler, Y., Marty, M., and Korup, O.: Regional snow-avalanche detection using object-based image analysis of near-infrared aerial imagery, Nat. Hazards Earth Syst. Sci., 17, 1823–1836, https://doi.org/10.5194/nhess-17-1823-2017, 2017.

Lato, M. J., Frauenfelder, R., and Bühler, Y.: Automated detection of snow avalanche deposits: segmentation and classification of optical remote sensing imagery, Natural Hazards and Earth System Sciences, 12, 2893–2906, https://doi.org/10.5194/nhess-12-2893-2012, 2012.

Leader, J.: The relationship between the Kirchhoff approach and small perturbation analysis in rough surface scattering theory, IEEE Transactions on Antennas and Propagation, 19, 786–788, 1971.

Leinss, S., Wiesmann, A., Lemmetyinen, J., and Hajnsek, I.: Snow water equivalent of dry snow measured by differential interferometry, IEEE J. Sel. Topics Appl. Earth Observ. Remote Sens., 8, 3773–3790, https://doi.org/10.1109/JSTARS.2015.2432031, 2015.

Leinss, S., Holenstein, S., and Wicki, R.: Sentinel-1 change detection mosaic of Switzerland for the avalanche event of January 4th 2018, https://doi.org/10.3929/ethz-b-000376048, 2019.

Matzler, C.: Microwave permittivity of dry snow, IEEE Transactions on Geoscience and Remote Sensing, 34, 573–581, 1996.

Meister, R.: Country-wide avalanche warning in Switzerland, in: Proceedings International Snow Science Workshop, Snowbird, Utah, USA, 30 October-3 November 1994, pp. 58–71, ISSW 1994 Organizing Committee Snowbird UT, USA, 1995.

MeteoSchweiz: Klimabulletin Januar 2018, Tech. rep., MeteoSchweiz, https://www.meteoschweiz.admin.ch/content/dam/meteoswiss/de/service-und-publikationen/Publikationen/doc/klimabulletin_januar_2018.pdf, 2018.

Rignot, E., Echelmeyer, K., and Krabill, W.: Penetration depth of interferometric synthetic-aperture radar signals in snow and ice, Geophysical Research Letters, 28, 3501–3504, https://doi.org/10.1029/2000GL012484, 2001.

Rudolf-Miklau, F., Sauermoser, S., Mears, A., and Boensch, M.: The Technical Avalanche Protection Handbook, Wiley, 2014.

Schweizer, J., Jamieson, J. B., and Skjonsberg, D.: Avalanche forecasting for transportation corridor and backcountry in Glacier National Park (BC, Canada), 25 Years of Snow Avalanche Research, Voss, Norway, 12-16 May 1998, pp. 238–243, 1998.

Schweizer, J., Kronholm, K., and Wiesinger, T.: Verification of regional snowpack stability and avalanche danger, Cold Regions Science and Technology, 37, 277 – 288, https://doi.org/https://doi.org/10.1016/S0165-232X(03)00070-3, http://www.sciencedirect.com/science/article/pii/S0165232X03000703, iSSW 2002: International Snow Science Workshop, 2003.

Scott, D.: Avalache Mapping: GIS for Avalanche Studies and Snow Science, The Avalanche Review, 27, 20–21, 2009.

SLF: Wochenbericht 05. Januar – 11. Januar 2018, https://www.slf.ch/de/lawinenbulletin-und-schneesituation/wochen-und-winterberichte/201718/wob-05-11-januar.html, 2018a.

SLF: Wochenbericht 12.–18. Januar 2018, https://www.slf.ch/de/lawinenbulletin-und-schneesituation/wochen-und-winterberichte/201718/wob-12-18-januar.html, 2018b.

SLF: Wochenbericht 19.–25. Januar 2018, https://www.slf.ch/de/lawinenbulletin-und-schneesituation/wochen-und-winterberichte/201718/wob-19-25-januar.html, 2018c.

SLF: Wochenbericht 26. Januar–01. Februar 2018, https://www.slf.ch/de/lawinenbulletin-und-schneesituation/wochen-und-winterberichte/201718/wob-26-januar-01-februar.html, 2018d.

SLF: Avalanche Bulletin, https://www.slf.ch/en/avalanche-bulletin-and-snow-situation.html#avalanchedanger, 2018e.

Small, D.: Flattening Gamma: Radiometric Terrain Correction for SAR Imagery, IEEE Transactions on Geoscience and Remote Sensing, 49, 3081–3093, https://doi.org/10.1109/TGRS.2011.2120616, 2011.

Small, D.: SAR backscatter multitemporal compositing via local resolution weighting, in: 2012 IEEE International Geoscience and Remote Sensing Symposium, pp. 4521–4524, https://doi.org/10.1109/IGARSS.2012.6350465, 2012.

Techel, F., Jarry, F., Kronthaler, G., Mitterer, S., Nairz, P., Pavšek, M., Valt, M., and Darms, G.: Avalanche fatalities in the European Alps: long-term trends and statistics, Geographica Helvetica, 71, 147–159, https://doi.org/10.5194/gh-71-147-2016, 2016.

Tiuri, M., Sihvola, A., Nyfors, E., and Hallikainen, M.: The complex dielectric constant of snow at microwave frequencies, IEEE Journal of Oceanic Engineering, 9, 377–382, https://doi.org/10.1109/JOE.1984.1145645, 1984.

Vickers, H., Eckerstorfer, M., Malnes, E., Larsen, Y., and Hindberg, H.: A method for automated snow avalanche debris detection through use of synthetic aperture radar (SAR) imaging, Earth and Space Science, 3, 446–462, https://doi.org/10.1002/2016EA000168, 2016.

Watte, W. P. and MacDonald, H. C.: Snowfield mapping with K-band radar, Remote Sensing of Environment, 1, 143 – 150, https://doi.org/https://doi.org/10.1016/S0034-4257(70)80016-5, http://www.sciencedirect.com/science/article/pii/S0034425770800165, 1970.

Werninghaus, R. and Buckreuss, S.: The TerraSAR-X mission and system design, Geoscience and Remote Sensing, IEEE Transactions on, 48, 606–614, https://doi.org/10.1109/TGRS.2009.2031062, 2010.

Wesselink, D. S., Malnes, E., Eckerstorfer, M., and Lindenbergh, R. C.: Automatic detection of snow avalanche debris in central Svalbard using C-band SAR data, Polar Research, 36, 1333 236, https://doi.org/10.1080/17518369.2017.1333236, 2017.

Wiesmann, A., Mätzler, C., and Weise, T.: Radiometric and structural measurements of snow samples, Radio Science, 33, 273–289, https://doi.org/10.1029/97RS02746, https://agupubs.onlinelibrary.wiley.com/doi/abs/10.1029/97RS02746, 1998.

Wiesmann, A., Wegmuller, U., Honikel, M., Strozzi, T., and Werner, C. L.: Potential and methodology of satellite based SAR for hazard mapping, in: IGARSS 2001. Scanning the Present and Resolving the Future. Proceedings. IEEE 2001 International Geoscience and Remote Sensing Symposium (Cat. No.01CH37217), vol. 7, pp. 3262–3264 vol.7, 2001.

Winkler, K., Zweifel, B., Marty, C., and Techel, F.: Schnee und Lawinen in den Schweizer Alpen, Hydrologisches Jahr 2017/18, WSL Berichte, 77, 2019.

Xu, X., Tsang, L., and Yueh, S.: Electromagnetic Models of Co/Cross Polarization of Bicontinuous/DMRT in Radar Remote Sensing of Terrestrial Snow at X- and Ku-band for CoReH2O and SCLP Applications, IEEE Journal of Selected Topics in Applied Earth Observations and Remote Sensing, 5, 1024–1032, 2012.